Fluorescence Spectroscopic Studies of (Acetamide + Sodium/Potassium Thiocyanates) Molten Mixtures: Composition and Temperature Dependence

Biswajit Guchhait, Harun Al Rasid Gazi, Hemant K. Kashyap, and Ranjit Biswas*

Department of Chemical, Biological and Macromolecular Sciences, and Unit for Nanoscience and Nanotechnology, S. N. Bose National Centre for Basic Sciences, Block-JD, Sector-III, Salt Lake, Kolkata-700098, India

Received: January 6, 2010; Revised Manuscript Received: February 13, 2010

Steady state and time-resolved fluorescence spectroscopic techniques have been used to explore the Stokes' shift dynamics and rotational relaxation of a dipolar solute probe in molten mixtures of acetamide (CH_3CONH_2) with sodium and potassium thiocyanates (Na /KSCN) at $T \sim 318$ K and several other higher temperatures. The dipolar solute probe employed for this study is coumarin 153 (C153). Six different fractions (f) of KSCN of the following ternary mixture composition, $0.75CH_3CONH_2 + 0.25[(1 - f)NaSCN + fKSCN]$, have been considered. The estimated experimental dynamic Stokes' shift for these systems ranges between 1800 and 2200 cm^{-1} (± 250 cm^{-1}), which is similar to what has been observed with the same solute probe in several imidazolium cation based room temperature ionic liquids (RTIL) and in pure amide solvents. Interestingly, this range of estimated Stokes' shift, even though not corresponding to the megavalue of static dielectric constant reported in the literature for a binary mixture of molten CH_3CONH_2 and NaSCN, exhibits a nonmonotonic KSCN concentration dependence. The magnitudes of the dynamic Stokes' shift detected in the present experiments are significantly less than the estimated ones, as nearly 40−60% of the total shift is missed due to the limited time resolution employed (full-width at half-maximum of the instrument response function ~70 ps). The solvation response function, constructed from the detected shifts in these systems, exhibits triexponential decay with the fastest time constant (τ_1) in the 10−20 ps range, which might be much shorter if measured with a better time resolution. The second time constant (τ_2) lies in the 70−100 ps range, and the third one (τ_3) ranges between 300 and 800 ps. Both these time constants (τ_2 and τ_3) show alkali metal ion concentration dependence and exhibit viscosity decoupling at higher viscosity in the NaSCN-enriched region. Time dependent rotational anisotropy has been found to be biexponential at all mixture compositions studied. Both the average solvation ($\langle\tau_s\rangle$) and rotation ($\langle\tau_r\rangle$) times of C153 in these mixtures exhibit *fractional* power law dependence on medium viscosity ($\langle\tau_x\rangle \propto \eta^p$, x being solvation or rotation). For solvation, p is found to be 0.46, which is very different from that obtained for common polar and nonpolar solvents, and RTILs ($p \approx 1$). For rotation, $p \approx 0.65$, which is again different from the value ($p \approx 1$) obtained for common polar solvents and RTILs but very similar to that ($p \approx 0.6$) found for nonpolar solvents. In addition, experimentally measured average rotation times in these mixtures are found to exhibit *slip* behavior in the low η/T region, which gradually transforms to *subslip* as η/T increases. Calculations using a recently developed semimolecular theory predict a total dynamic Stokes' shift for C153 (dipolar solute) in these molten mixtures near ~1600 cm^{-1} where the solute−solvent (dipole−dipole) and the ion−solute (ion−dipole) interactions contribute respectively ~80% and ~20% to the calculated total shift. Like in experiments, the theoretically predicted solvation response function in the *overdamped* limit at each mixture composition has been found to be triexponential. The calculations in the *underdamped* limit, however, suggest a biphasic decay where a composition independent subpicosecond component and a much slower component with the time constant spreading over 150−850 ps contribute equally to constitute the total decay. The calculated average solvation times in this limit are found to be in better agreement with experimental results than the predictions from the overdamped limit.

I. Introduction

Acetamide, upon melting at around 353 K (boiling point ~495 K), forms a fairly mobile liquid (viscosity, $\eta \sim 2.2$ cP) and has long been known for its exquisite solvent properties.[1–5] The presence of several functional groups such as methyl, carbonyl, tautomeric hydroxyl, and amide groups in the same molecule render strong solvating power to this compound for a very large number of organic and inorganic substances except cellulose.[1] The high dielectric constant of molten acetamide ($\varepsilon_0 \approx 60$) coupled with its large dipole moment (3.7 D) makes it an even better solvent than water for many ionic compounds.[4] Since addition of inorganic salts lowers the melting temperature of acetamide considerably, molten binary and ternary mixtures of acetamide with metal halides have been used as reaction media and also in thermal salt cells to produce electricity.[6,7] The possibility of using acetamide as a suitable medium for electrodeposition of metals from salt solutions has also been investigated.[2] Several other aspects such as ion conductance[5] and micellization of surfactants in molten acetamide have been studied by several authors to understand the role of the

* Corresponding author. E-mail: ranjit@bose.res.in.

10.1021/jp1001176
Published on Web 03/29/2010

ion−solvent interactions in controlling the ion transport and self-aggregation in this medium.[8–13]

Because of industrial applications of molten acetamide as nonaqueous solvents for electrolytes and possible use in supercapacitor technology, the liquid−solid equilibrium temperature of (acetamide + electrolyte) mixtures has been explored extensively.[14–25] These studies reveal that mixtures of acetamide with certain electrolytes produce liquids that supercool (no spontaneous crystallization) until the glass transition temperature (T_g) is reached. Furthermore, the phenomenon of supercooling depends on the nature of the ion present in the mixture and Na^+ is found to produce the strongest supercooling effect. It is therefore evident that a stronger ion−acetamide interaction (relative to the ion−ion and acetamide-acetamide interactions) inhibits the phase separation and leads to the supercooling of the molten mixture. Viscoelastic,[22,23] dielectric,[24,25] and nuclear magnetic[22] relaxation studies of fused (acetamide + NaSCN) mixtures at temperatures above T_g have all indicated microscopic heterogeneity in the liquid structure. The observed multiple relaxation processes are subsequently explained in terms of an equilibrium between ordered (salt induced polymerized acetamide) and disordered solvent domains.[15a,b] In addition, dielectric relaxation measurements of fused acetamide in the presence of NaSCN at 0.225 mol fraction ($T_g \sim 230$ K) report the megavalue (10^6) of the static dielectric constant (ε_0) at $T \approx 274$ K. Such a high value of static dielectric constant of this mixture has been explained in terms of highly cooperative alignment of dipoles forming extended ordered domains.[25]

The formation of ordered domains and types of interactions present in these molten mixtures provide these systems kinship to the room temperature ionic liquids (RTILs) where solution heterogeneity and longer-ranged interactions govern much of the solvent properties.[26–32] In addition to these, when one also considers the reported megavalue of the static dielectric constant,[24] one cannot but wonder what would be the overall medium effects on fluorescence Stokes' shift and its dynamics of a dipolar probe dissolved in these molten mixtures.[33] Moreover, a significant slow component[34–38] in the Stokes' shift dynamics is expected as the relevant dielectric relaxation (DR) measurements ($T \sim 310$ K)[24] report relaxation times in the milliseconds and nanoseconds for the low (0.1−100 Hz) and high (100 to 10^8 Hz) frequency dispersions, respectively. However, a large fraction of the total dispersion at higher frequency range ($\Delta\varepsilon = \varepsilon_\infty - n^2$, n being the refractive index of the medium) has remained inaccessible as these measurements could reach the infinite frequency dielectric constant (ε_∞) only up to ∼18. Since the fast component of the orientational dynamics of a polar medium is naturally contained in this high frequency dispersion component,[39–42] no information regarding the fast dynamics of these molten mixtures can be obtained from these incomplete DR data. Surprisingly, even simple fluorescence spectroscopic measurements for these systems have not been done yet and, as a result, nothing is known about solute−solvent interaction in these multicomponent molten mixtures.

The above scenario has motivated us to carry out dynamic fluorescence Stokes' shift and anisotropy measurements of a dissolved dipolar probe (coumarin 153, abbreviated as C153) in molten mixtures of acetamide (CH_3CONH_2) with potassium thiocyanate (KSCN) and sodium thiocyanate (NaSCN) at six different fractions (f) of KSCN, with mixture composition, $0.75CH_3CONH_2 + 0.25[(1 - f)\text{NaSCN} + f\text{KSCN}]$ at T (K) ∼318. Note that study of liquid−solid equilibrium temperature for mixtures of CH_3CONH_2 with either NaSCN or KSCN has indicated[15] *eutectic* temperatures (T_u) around 300 K at thiocyanate mole fraction ∼0.2. A much closer look at these results[15] will reveal that the mole fraction of CH_3CONH_2 considered in the present study (0.75) actually allows one to investigate the solute−medium interaction on either side of the T_u where the mixture remains in a single (liquid) phase. The choice of temperature then decides the proximity of the mixture to the solid−liquid phase separation line and the consequent effects. The fraction (f) of KSCN in these mixtures is varied in the present study to convert the system from binary mixtures ($f =$ 0 and 1) to ternary ones so that the mixed alkali effects (MAE)[43–49] on fluorescence dynamics can be investigated. It is interesting to note that the MAE, which corresponds to deviation of various physical properties from the mole-fraction-weighted additivity at a given temperature when one alkali metal ion is continuously replaced by another in a glass or melt, are not generally reflected in the equilibrium properties but show up in transport properties, such as, electrical conductivity and viscosity.

Since both the solvation and rotational dynamics of a dipolar solute probe would be substantially affected by the ion motions (independent or correlated) and medium viscosity, it would be worthwhile to investigate the MAE on average solvation and rotation times in these molten mixtures. The choice of this system is further motivated by the fact that density and viscosity of this mixture as a function of KSCN fraction have already been studied for a reasonably large temperature range.[44] These studies have revealed significant MAE for the composition dependent viscosity where a Vogel−Fulcher−Tammann (VFT) type of description has been found to be suitable for the temperature dependence of viscosity in these mixtures.[44] For the sake of completeness, we present in Figure S1 (Supporting Information) a plot of solution viscosity as a function of KSCN concentration, measured at ∼318 K.[44] Note also that the molten mixtures at six different fractions of KSCN considered here at 318 K are always in the liquid phase and far away from the respective glass transition temperatures. In addition, temperature dependencies (318−375 K) of the average rotation times at two KSCN fractions (f = 0.2 and 0.8) have been studied to investigate further into the solute−environment interaction in these complex mixtures. Such a study for solvation dynamics in these mixtures has also been attempted, but meaningful results could not be obtained due to Stokes' shift dynamics becoming too fast at higher temperatures to be detected by the limited time resolution employed in the present experiments.

The rest of the paper is structured as follows. Experimental details regarding sample preparation, data collection and their analysis methods have been described in the next section. Section III contains results of our measurements and subsequent discussion. Comparison with theoretical predictions (wherever possible) has also been made in this section. The theoretical model and equations necessary for calculations of the Stokes' shift and its dynamics in these molten mixtures have been described in the Appendix. The paper then ends with concluding remarks provided in section IV.

II. Experimental Details

A. Sample Preparation. Laser grade C153 was purchased from Exciton and used without further purification. Acetamide (≥99%, SRL, India), sodium thiocyanate (≥99%, SRL, India), and potassium thiocyanate (≥98%, Merck Specialties, India) were vacuum-dried (∼300 K) overnight before use. Samples were prepared by quickly transferring the required amounts of each of these compounds in proper volumetric flasks at a given composition at room temperature. No inert gas atmosphere was

used during weighing and transferring the individual components of these mixtures. Each of the samples (in volumetric flasks) was then heated carefully using a water bath to about 325 K (Julabo, model F32) to melt the samples. An aliquot (~3 mL) of this stock melt was then transferred into a preheated quartz cuvette (path length 1 cm), which was previously loaded with C153 grains, and sealed. C153 loading was done via taking ~5 μL of a stock solution of C153 in heptane and drying by heating the outer surface of the cuvette with mildly hot air and gently passing dry N_2 gas into the cuvette. The concentration of C153 in the stock C153/heptane solution was such that the final concentration of the probe (C153) in molten mixtures was always maintained at $\leq 10^{-5}$ M. The properly sealed (using Teflon tape) sample cuvette (cuvette containing the molten mixture and C153) was then shaken gently for ~5 min and dipped into the water bath for ~10 min (maintained at 318 ± 0.5 K). This process was repeated for a number of times before transferring the sample cuvette into the sample chamber of a spectroscopic instrument. A wait time of ~15 min was observed after loading the sample cuvette into the temperature-maintained sample chamber of each of the spectrometers before data collection. A few samples (randomly chosen) were bubbled with dry N_2 gas before data collection but did not show any difference with those collected with the unbubbled samples.

B. Spectral Data Collection and Analyses for Solvation Dynamics Studies. Steady state absorption (UV-2450, Shimadzu) and fluorescence (Fluoromax-3, Jobin-Yvon, Horiba) spectra were collected, solvent back-ground corrected, and converted properly to the frequency domain before analyzing the spectra for further use. Time-resolved fluorescence measurements were carried out using the time correlated single photon counting technique based on a laser system (LifeSpec-ps, Edinburgh Instruments, U.K.) that provided 409 nm light as an excitation source. All data were collected with a band-pass of ±2 nm where the temperature of the sample chamber was maintained at 318 ± 0.5 K. The full width at half-maximum (fwhm) of the instrument response function (irf) measured using distilled water as a scattering medium and 409 nm excitation light was found to be ~70 ps.

For solvation dynamics studies, we collected at magic angle 18−20 decays at equally spaced wavelengths across the steady state emission spectrum of C153 (solute) dissolved in these molten mixtures. Decay collection at each of these wavelengths was continued until the peak count was reached ~5000 (dark count ~10). This provided reasonably good statistics in the subsequent fitting of the collected decays. The collected emission decays were first deconvoluted from the irf to remove the instrumental broadening and then fitted with a multiexponential function using an iterative reconvolution algorithm.[33,50] Such a fitting procedure is known to sharpen the effective time resolution by a factor of ~3−4,[33,50–53] and therefore, time scales in the ~15−20 ps range generated from decay fits in the present study may indicate the presence of such dynamics or even much faster ones in these molten mixtures. Although the relatively faster components might be completely missed due to such a resolution, the long time dynamics is expected to be detected rather well. Time-resolved emission spectra (TRES) were then reconstructed from the decay fit parameters in conjunction with normalized intensities at each of these wavelengths of the steady state emission spectrum.[54] The time dependent solvation of the laser excited probe was then followed by constructing the normalized spectral or solvation response function[33]

$$S(t) = \frac{\nu(t) - \nu(\infty)}{\nu(0) - \nu(\infty)} \quad (1)$$

where $\nu(x)$ denotes some measure (first moment or peak) of the time-resolved emission spectrum at various time slices. While $\nu(0)$ represents the frequency of the dissolved solute's emission spectrum immediately after excitation when the solvent relaxation has not started yet but the vibrational relaxation in the solute is assumed to be complete, $\nu(\infty)$ is the frequency of the emission spectrum after the solvent relaxation is complete (the solute is still in its excited state).[55] It is therefore expected that the fluorescence emission spectrum at $t = \infty$ obtained from the time-resolved experiments should be the same as that obtained from the steady state experiments. However, the *average*[56] peak frequency of the time-resolved spectrum extrapolated at $t = \infty$ ($\nu(\infty)$) was found to be red-shifted by ~300−600 cm^{-1} (±250 cm^{-1}) in comparison to that of the steady state fluorescence emission spectrum. This is somewhat larger than what was found in several RTILs[57] and indicates that for some nonzero KSCN fractions, the steady state fluorescence emission spectrum did not arise from the fully solvent-relaxed excited state. More importantly, this small but non-negligible fraction (~15−30%) of the estimated total dynamic Stokes' shift[58,59] is associated with the slowest component of the total spectral relaxation and thus strongly affects the magnitude of the average solvation time, $\langle \tau_s \rangle = \int_0^\infty dt\, S(t)$. As the experimentally obtained solvation response function, $S(t)$ at each of these mixtures was found to be multiexponential functions of time, the average solvation times were obtained analytically as $\langle \tau_s \rangle = \sum_{i=1}^{n} a_i \tau_i$.

C. Data Collection and Analyses for Time-Resolved Fluorescence Anisotropy, *r(t)*. Emission decays for time-resolved anisotropy studies were collected at the peak wavelength of steady state emission bands to minimize the effects (if any) on anisotropy of fast decay or rise due to solvent reorganization.[60,61] A set of three decays, namely, the vertically ($I_{||}$), horizontally ($I_\perp$), and magic angle polarized emissions (with respect to the sample being excited with the vertically polarized light) were recorded. The magic angle decay was first deconvoluted from the irf and fitted to multiexponential function of time. Subsequently, the parallel ($I_{||}$) and the perpendicular ($I_\perp$) decays were simultaneously fitted by using an iterative reconvolution algorithm[62] to construct the time-resolved fluorescence anisotropy

$$r(t) = \frac{I_{||}(t) - GI_\perp(t)}{I_{||}(t) + 2GI_\perp(t)} \quad (2)$$

where the longest lifetime obtained from the magic angle decay fit was used during the fit. The geometric factor (G) was obtained by tail matching the intensity decays, $I_{||}(t)$ and $I_\perp(t)$, at time longer than the anticipated rotation time. The time-resolved anisotropy, thus constructed for each of the mixtures studied here, was found to be adequately described by a sum of two exponentials of the following form

$$r(t) = r(0)[a_1 \exp(-t/\tau_1) + a_2 \exp(-t/\tau_2)] \quad (3)$$

where $a_1 + a_2 = 1$ and τ_1 and τ_2 are the two time constants associated respectively with decay amplitudes a_1 and a_2. $r(0)$ denotes the initial anisotropy and for C153 it was taken as 0.38 in all the molten mixtures studied here.[60] The average rotational

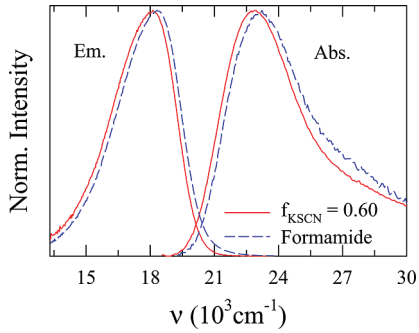

Figure 1. Steady state absorption and fluorescence emission spectra (color coded) of C153 (solute) dissolved in a molten mixture at f_{KSCN} = 0.60 (318 K) and in formamide at room temperature. Note that the blue tails in the absorption spectra might have originated from the improper functioning of the instrument at shorter wavelengths and thus would be unrealistic. However, this does not affect the overall observation and final conclusions made in this paper. Similar comparison with molten acetamide is not done because the ion−solute interaction contribution to the spectral shift in these mixtures is expected to be covered by the relatively larger average dielectric constant of formamide at room temperature (ε_0 = 111).

correlation time, $\langle\tau_r\rangle$, was then obtained via integrating the normalized function, $r(t)/r(0)$, and thus calculated analytically as, $\langle\tau_r\rangle = a_1\tau_1 + a_2\tau_2$.

III. Results and Discussion

A. Steady State Spectroscopic Studies. Representative steady state absorption and fluorescence emission spectra of C153 dissolved in a molten mixture of composition, $0.75CH_3CONH_2 + 0.25[(1 - f)NaSCN + fKSCN]$, at ~318 K with $f_{KSCN} = 0.6$ are shown in Figure 1. Absorption and emission spectra of C153 in pure formamide (FA) at ~298 K are also shown in the same figure (blue) for comparison. Note in Figure 1 the similarity in spectral position and shape between the absorption and emission spectra in ternary mixture and those in FA. More quantitatively, the *average* absorption and emission spectral peak frequencies[63] for C153 in this mixture are found to be respectively (in the unit of 10^3 cm^{-1}) 23.62 and 17.73, whereas those in FA are 23.91 and 17.96. The spectral widths (full width at half-maximum, fwhm) are also very close in these two media (in the unit of 10^3 cm^{-1}): for absorption, 4.43 in this mixture versus 4.77 in FA and, for emission, 3.48 (molten mixture) versus 3.44 (FA). As a result, the steady state Stokes' shifts (relative to that in heptane[63]) in these two media are very similar, ~1450 cm^{-1} in molten mixture and ~1500 cm^{-1} in FA. The closeness of the spectral data therefore clearly indicate that the net interaction between the solute and the surrounding environment in this molten mixture is very similar to that in FA. This is somewhat surprising because a much greater difference with FA is expected on the basis of the extremely large (~10^6) static dielectric constant reported earlier[24] for a molten mixture of acetamide with sodium thiocyanate at T ~ 310 K. Furthermore, similar spectral widths (both absorption and emission) in the molten mixture and FA is also intriguing considering the fact that various studies with such molten mixtures have already suggested the presence of strong heterogeneity in the solution phase.[22−25]

In fact, the similarity of spectral data between the molten mixture and FA has also been observed for other compositions as well. This is shown in Figure 2 where peak frequencies of absorption and emission spectra obtained at six different fractions of KSCN are shown along with the spectral widths (fwhm) and relative steady state Stokes' shifts. Note in the upper

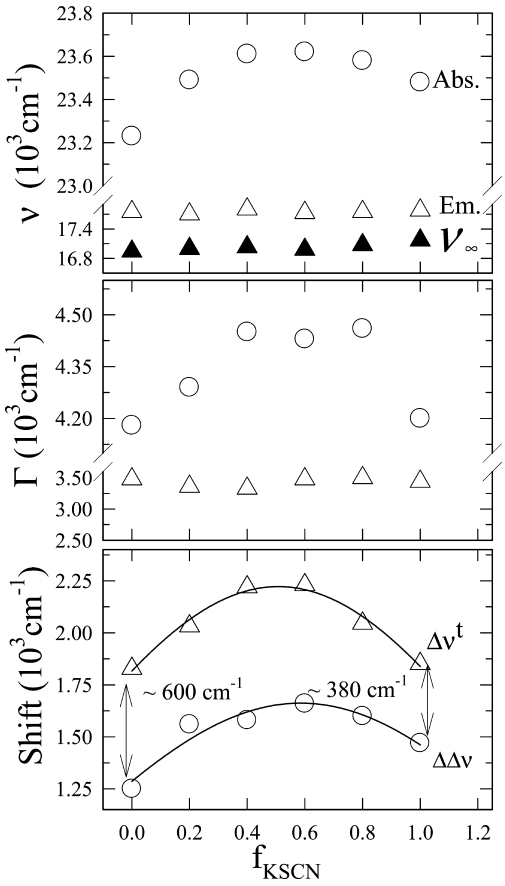

Figure 2. Spectral data in six different fractions of KSCN: Concentration dependencies of absorption and emission peak frequencies (ν) are shown in the upper panel and those for full width at half maxima (Γ) and Stokes' shifts (steady state and dynamic) are presented respectively in the middle and bottom panels. ν_∞ shown in the upper panel represents emission peak frequencies obtained at $t = \infty$ from time-resolved experiments. $\Delta\nu^t = \nu(t = 0) - \nu(t = \infty)$ and $\Delta\Delta\nu = [\nu_{abs} - \nu_{em}]^{mixture} - [\nu_{abs} - \nu_{em}]^{heptane} = \Delta\nu^{mixture} - \Delta\nu^{heptane}$. $\nu(t = 0)$ has been estimated by using the Fee−Maroncelli method[58] and $\Delta\nu^{heptane}$ is measured as 4230 cm^{-1}.

panel that while the absorption peak frequency shows a nonmonotonic (though not very strong) KSCN concentration dependence, the emission frequencies remain almost independent to the variation of KSCN concentration. The apparent insensitivity of the emission peak frequency to the KSCN concentration in the ternary mixture does not indicate that the solvation environments around the solute in its ground and excited states are different. The slow movement of ions and other ion−solvent composite species present in these viscous mixtures (see Figure S1 (Supporting Information) for viscosity range) may lead the fluorescence emission to take place from not a fully solvent-relaxed excited state. This might be particularly true for the more viscous NaSCN-rich region where Na^+ is believed to induce pronounced solvent polymerization.[15b] This means that in this (NaSCN-rich) region the emission frequencies are probably "blue-shifted" compared to what should have been, had emission taken place from a completely solvent-relaxed state. Such a "blue shift" of spectral frequency has also been observed earlier for electrolyte solutions of multivalent ions in pure polar solvents.[52,59] The fluorescence emission frequency obtained after extrapolating the time-resolved emission spectra to infinite time ($\nu_{em}(t = \infty)$, shown by filled triangles) at each fraction of KSCN seems to indicate that the steady state emission in these mixtures has taken place from an incompletely solvent-relaxed excited state of the dissolved solute.

Spectral widths of absorption and emission spectra of C153, shown in the middle panel of Figure 2, also vary with KSCN concentration much the same way as the respective spectral peak frequencies. It is interesting to note here that in the NaSCN-rich region the absorption spectrum blue-shifts and broadens while it red-shifts and narrows in the KSCN-rich region. Even though both the spectral shift and width variation are small and limited to ≤ 300 cm^{-1}, the effect of replacement of Na^+ ion by the K^+ ion on solute absorption spectrum is evident. In addition, the correlation between the spectral shift and width seen here is very different from those observed earlier[33] in common polar solvents where broadening of the spectrum (absorption) associates with a red shift and narrowing with a blue shift. However, a red shift with narrowing in the absorption spectrum has been observed earlier with C153 and other solutes at very low alcohol concentrations in binary mixtures of water with tertiary butanol (TBA) and ethanol.[53,64] In these works, a novel interplay between solution polarity and association among alkyl groups of alcohol molecules has been suggested to be responsible for the red shift with concomitant narrowing of the absorption spectrum. A plausible explanation for the correlation between the spectral shift and width observed in these molten mixtures can be constructed as follows. As Na^+ is increasingly replaced by K^+ in the ternary mixture, the packing becomes less effective due to the resultant size constraint (size of K^+ is larger than that of Na^+).[42] The less effective packing around the solute then leads to a blue shift of the absorption spectrum. Also, the additional presence of K^+ enhances the heterogeneity, leading to an increase in the spectral width. Further addition of KSCN decreases the relative concentration of Na^+ in the mixture which, in turn, enhances the solute−solvent direct interaction by reducing the degree of solvent polymerization[15] and structural heterogeneity. Consequently, a red shift (relative to that at $f_{KSCN} \approx 0.5$) with concomitant narrowing is observed in the solute's absorption spectrum. Therefore, several factors, such as, packing of ions around the dissolved solute, heterogeneity in solution structure due to presence of different kind of ions, and polymerization of acetamide due to the presence of alkali metal ions[15] could be responsible for the observed dependence of spectral properties on salt concentrations in these molten mixtures.

The nonmonotonicity in absorption peak frequency dependence also gives rise to the nonmonotonic alkali metal ion (K^+ or Na^+) concentration dependence of the steady state Stokes' shift (relative to heptane) in these mixtures. This is shown in the bottom panel of Figure 2 where the Stokes' shifts obtained after replacing the steady state emission frequency (ν_{em}) by the emission frequency extrapolated at $t = \infty$ from time-resolved experiments ($\nu_{em}(t = \infty)$) are also presented. Note that the relative shift calculated by using $\nu_{em}(t = \infty)$ is essentially the dynamic Stokes' shift measured in solvation dynamics experiments.[65] Interestingly, both the steady state and dynamic Stokes shifts go through maxima when plotted as a function of alkali metal ion concentration. Several transport properties, such as electrical conductivity and viscosity, of these mixtures also exhibit similar nonmonotonic ion concentration dependences and have been explained in terms of what is known as mixed alkali effects.[10,44] Another important aspect of these data is that the estimated dynamic Stokes' shifts are larger by $\sim 300-600$ cm^{-1} than the steady state values observed earlier for strongly polar solvents with the same solute at ambient condition.[33] Therefore, whether a difference between steady state and dynamic shifts of ~ 300 cm^{-1} in the KSCN-rich region and ~ 600 cm^{-1} in the NaSCN-rich region is a consequence of slow (relative to the excited state lifetime of the probe) environmental rearrangement or actually emerges from the subtle modifications in the underlying vibronic structure of the spectral line-shape in these mixtures at different compositions cannot be ascertained at this moment without further study.

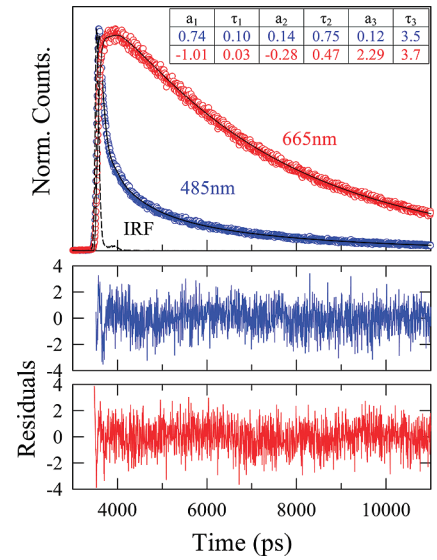

Figure 3. Representative fluorescence intensity decay of C153 at blue and red wavelengths at $f_{KSCN} = 0.60$ for a molten mixture ($T \sim 318$ K). Experimental data are shown by circles, and fits through them, by solid lines. The instrument response function is also shown in the same figure (dashed lines). The respective residuals (color coded) are presented in the bottom panels. The fit parameters are shown in the inset of the upper panel. The time constants (τ_i) are in nanoseconds.

B. Time-Resolved Fluorescence Spectroscopic Studies. Typical fluorescence emission intensity decays collected at the blue (485 nm) and red (665 nm) end of the steady state emission spectrum of C153 dissolved in the ternary mixture at $f_{KSCN} = 0.6$ and 318 K are shown in Figure 3. Multiexponential fits through these decays, fit parameters, and instrument response function are also shown in the same panel (upper panel). As suggested by the fit parameters and nonregular pattern in the residuals (shown in the bottom panel), triexponential functions are adequate to describe the time-resolved emission decays at these wavelengths. Note that for decays collected at and around the peak wavelengths of the corresponding emission spectrum, biexponential functions of time have been found to be sufficient. The decay characteristics at these wavelengths (rise followed by decay at the red end and decay only at the blue end) clearly indicate rearrangement of the environment in response to the instantaneously altered dipole moment of the solute dissolved in these molten mixtures. A point for concern is, however, that whether, in addition to the spectral relaxation, dynamic quenching of the fluorescence also contributes to the total decay in these mixtures. This we have checked by following the alkali metal ion concentration dependence of the longest time constant found in the fits of the collected emission intensity decays (see Figure S2, Supporting Information). If the longest time constants (τ_2 for biexponential and τ_3 for triexponential fits) are identified with the excited state lifetime (τ_{life}) of the fluorescent probe, then data shown in Figure S2 do not reflect any drastic modification (no more than $\sim 6\%$) of the probe's "lifetime" across the entire range of KSCN concentration in these molten mixtures. In addition, no significant intensity change has been detected in the controlled steady state spectroscopic experiments with these mixtures. Therefore, the decay components observed at this and other KSCN fractions may be considered as

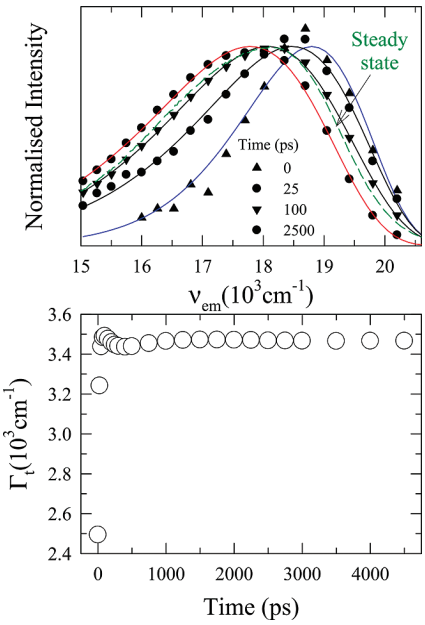

Figure 4. Synthesized time-resolved emission spectra (TRES) of C153 in a ternary molten mixture at $f_{KSCN} = 0.60$ at various time intervals. The data representations are as follows: 0 (triangle), 25 (diamond), 100 (inverted triangle), and 2500 (circle) ps after solute excitation at ~318 K (upper panel). Spectral widths of the TRES are shown in the bottom panel.

associated with the time dependent solvation of the laser-excited probe in these molten mixtures.

Representative time-resolved emission spectra (TRES) of C153 in ternary molten mixture at $f_{KSCN} = 0.6$ and ~318 K are shown in the upper panel of Figure 4. The lines going through the points are obtained from fitting the reconstructed data points to a log-normal line shape function.[54] The difference (peak to peak) between the reconstructed time-zero spectrum and that at $t = \infty$ is found to be ~1300 cm^{-1}, which is nearly 40% less than the estimated "true" dynamic Stokes' shift ($\Delta\nu^t_{est} \approx 2200$ cm^{-1}) for C153 in this mixture. The steady state emission spectrum of C153 in this mixture at this temperature is also shown in the same panel. Note that the steady state emission spectrum is "blue-shifted" ~400 cm^{-1} relative to the time-resolved emission spectrum at $t = \infty$. It is already discussed that this has been typical for these molten mixtures, which originates probably either from the sluggish movement of solvent and/or ion−solvent composite species or from the subtle changes in the vibronic structure of the spectrum. More importantly, the overall spectral shape of the time-resolved spectrum obtained at different time slices does not change with time. Also, the width, shown in the bottom panel, changes very little (except for spectrum at "$t = 0$") with time. The use of broader time resolution in the present experiments and consequently poor fitting of the data points for the time-resolved spectrum at "$t = 0$" are probably the reasons for the relatively smaller width of the time-zero spectrum. If this small inconsistency for the time-zero spectrum is ignored, then the widths of the time-resolved emission spectra lie roughly in the range 3400 ± 200 cm^{-1} which is very similar to those of steady state emission spectra of C153 in this molten mixture and in ambient pure formamide. Therefore, the total end-to-end variation in spectral width (~400 cm^{-1}) is much smaller than the detected or estimated shift in this mixture and closely resembles to the findings in ionic liquids[57] and common dipolar solvents.[33] As near insensitivity to time of spectral shape and width is a hallmark for the measurement of nonreactive solvent dynamics in bulk liquids by using a solvatochromic probe, the spectral evolution presented in this figure (Figure 4) can be considered as reflecting the medium-induced dynamic Stokes' shift in these complex molten systems.

TABLE 1: Dynamic Stokes' Shift for C153 in Molten Mixtures of Acetamide with Na^+/K^+ Thiocyanates at ~318 K: Comparison between Theory and Experiments

	theory			experiment		
f_{KSCN}	ν^t_{sd} (cm^{-1})	ν^t_{si} (cm^{-1})	ν^t_{total} (cm^{-1})	ν^t_{est} (cm^{-1})[a]	ν^t_{obs} (cm^{-1})	% missed
0.0	1262	328	1590	1828	1082	41
0.2	1260	331	1591	2032	910	55
0.4	1259	335	1594	2120	981	54
0.6	1258	339	1597	2230	1337	40
0.8	1256	343	1599	2045	1046	49
1.0	1255	347	1602	1851	791	57

[a] The estimated shifts are obtained by using the Fee−Maroncelli method described in ref 58. The error bar associated with the measurements is approximately ±250 cm^{-1}.

Dynamic Stokes' shifts measured ($\Delta\nu^t_{obs}$) for other KSCN concentrations at ~318 K are summarized in Table 1 where the estimated shifts ($\Delta\nu^t_{est}$) are also tabulated to show the amount missed in the present studies of solvation dynamics in these mixtures. Data in the last column of Table 1 suggest that the relevant experiments have failed to detect nearly half of the total shifts in these molten mixtures. This indicates the existence of solvent dynamic components in these molten mixtures which are, *at least*, 3−4 times faster than the time resolution (~70 ps) employed in these measurements. We shall discuss more about it when we present results on solvation dynamics in these systems as missing of faster components poses a serious difficulty for ascribing physical origin to the observed time scales. We now focus on whether the shifts estimated for C153 at various KSCN concentrations in these mixtures can be described, even qualitatively, by a theory in terms of interactions of the dipolar solute with the dipolar component (acetamide) and the ions (Na^+, K^+, and SCN^-) present in the system.

Since the molten mixtures of acetamide with sodium and/or potassium thiocyanates represent nonaqueous electrolyte solutions, the total dynamic Stokes' shift in these media may be assumed to be composed of the following: contributions from the dipole−dipole interaction between the dipolar solvent and the dipolar solute, and the dipole−ion interaction between the dipolar solute and the ions. Such an electrolyte solution model has recently been found to be very successful in predicting not only the measured Stokes' shift in several ionic liquids but also the observed dynamics in them.[66] As a detailed discussion on the calculation of dynamic Stokes' shift based on electrolyte solution model has already been provided in ref 66 and also presented briefly in the Appendix of this paper, we just show the calculated shifts here and compare with the experimental estimates. The calculated shifts are also summarized in Table 1 where the dipole−dipole interaction contribution ($\Delta\nu^t_{sd}$) at various values of f_{KSCN} are presented in the second column, dipole−ion ($\Delta\nu^t_{si}$) in the third and the total ($\Delta\nu^t_{total}$) in the fourth. Note that in the absence of any systematic conductivity measurements for these systems, the salts are assumed to be completely dissociated. The polar solvent (acetamide) is assumed to be a collection of dipolar hard spheres each possessing a dipole moment (μ_d) of 3.7 D. This value of dipole moment produces an average static dielectric constant (ε_0) as ~30 for the solvent composed of dipolar hard spheres. The solute's size and dipole moments are taken as those of a C153 molecule.

The KSCN fraction dependent static dielectric constant of the medium (ε_0) is calculated from the experimental density by using the mean spherical approximation (MSA) theory.[67] In addition, the ions are approximated as hard-sphere ions where the size disparity between cations has been neglected. Therefore, the theory reduces to that for a binary mixture of acetamide with a uniunivalent electrolyte in it where the effects of change in KSCN concentration enter in the calculation only via the use of experimental density. As a result, ion-specific effects (for example, difference in solvent polymerization[15] and packing ability) on dynamic Stokes' shift would be completely missing in the predicted results. Also, the predicted shift would be nearly constant regardless of the changes in KSCN concentration, as the density of the molten mixture does not change significantly with the fraction of KSCN (see Table S3 in the Supporting Information).

A notable aspect of the comparison between the calculated total ($\Delta\nu^t_{total}$) and experimentally estimated ($\Delta\nu^t_{est}$) shifts for C153 in these molten mixtures is that the predicted shifts are in general agreement with the estimated ones. Note also that the contribution due to the interaction of the dipolar solute with the surrounding ions ($\Delta\nu^t_{si}$) is only about 20% of the total shift. The ion−dipole interaction contribution ($\Delta\nu^t_{si}$) is thus smaller compared to the prediction for imidazolium ionic liquids[66] but close to what has been observed for electrolyte solutions in strongly polar solvents at room temperature.[50] Even though the calculated total shifts are ∼300−600 cm^{-1} less than the estimated values, the closeness in the agreement suggests that the present calculation scheme possesses a certain degree of validity even for these complex ternary mixtures. More importantly, the level of agreement achieved here corresponds to an electrolyte solution in a model solvent of average dielectric constant ∼30, which is *insignificant* compared to the reported huge value of ε_0 for the (CH_3CONH_2 + NaSCN) mixtures.[24] This clearly indicates the inaccuracy in the reported dielectric relaxation measurements[24] and also explains why the steady state spectra in these mixtures closely resemble to those in formamide at room temperature (see Figures 1 and 2).

Representative decay of the spectral or solvation response function, $S(t)$, obtained from the time-resolved emission spectra are shown in the upper panel of Figure 5 for three different fractions of KSCN in the molten mixture at ∼318 K. Note that the decay becomes faster upon increasing the fraction of KSCN (f_{KSCN}) in the mixture. This correlates well with the concomitant decrease in solution viscosity. Solvation response functions obtained by using two different measures of spectral frequency—the first moment (solid line) and the peak (broken lines)—are compared in the lower panel. These results suggest that, like in dipolar solvents,[33] spectral movement with time is rather uniform, which makes the decay largely insensitive to the choice of the frequency measure for constructing the $S(t)$. The decays shown in this figure as well as those obtained at other KSCN fractions have been found to fit to triexponential functions of time, producing time constants in the tens, hundreds, and a few to several hundreds of picoseconds regimes. The fit parameters (amplitudes and time constants) describing $S(t)$ and the corresponding average solvation time at each of the KSCN fractions studied are summarized in Table 2 along with the corresponding viscosity values. Although the fastest time constant (τ_1) is too short compared to the detection limit in the present experiments, the recurrent occurrence of it in each of the KSCN fractions indicate the presence of a very fast component in the overall solvation response in these molten mixtures. Note that the other two time constants do not change much (varies within ±5% of the reported values) even if the fastest time constant (τ_1) is fixed during fitting of the spectral response functions. The presence of low frequency (∼100 cm^{-1}) intermolecular libration bands in amide systems[68] and their relation to the ultrafast solvation energy relaxation in these[39−42,66] and other hydrogen-bonded solvents[69,70] have made an ultrafast solvation component (time constant ∼1 ps or even faster) a distinct possibility for these molten acetamide and salt mixtures. We shall explore further on the origin of this time scale when we present model calculations on solvation dynamics in these mixtures. Interestingly, the other two time constants (τ_2 and τ_3) are roughly in the ranges of what was observed earlier for biphasic solvation response of C153 in one component molten inorganic salts at elevated temperatures.[71] While those studies have indicated a correlation between the ion size and time constant without providing any quantitative information on the viscosity of the molten media, a clear correlation between the relatively larger time constants (τ_2 and τ_3) and solution viscosity can readily be seen in the present study. However, for these molten mixtures the following questions still remain to be answered. First, is it the ion-translation or dipolar solvent rotation or, a combination of both responsible for the larger time constants (τ_2 and τ_3) in these multicomponent mixtures? Second, what role do the low frequency intermolecular collective librational modes of acetamide play in determining the time scale of solvation energy relaxation at early times in these systems? Below we elaborate

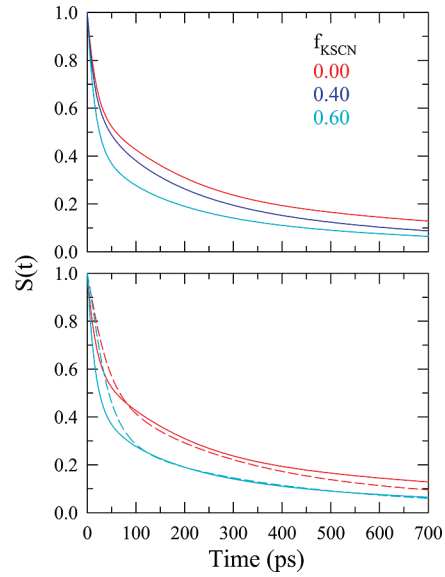

Figure 5. Representative decays of solvation response function, $S(t)$ at three different KSCN fractions (upper panel) and comparison of $S(t)$ decays obtained from first moment (solid lines) and the peak (broken lines) frequencies (bottom panel) for two different KSCN fractions. The representations are color coded.

TABLE 2: Experimentally Measured Solvation Response Functions at Different Mixture Compositions at ∼318 K: Fit Parameters[a]

f_{KSCN}	viscosity (cP)	a_1	τ_1 (ps)	a_2	τ_2 (ps)	a_3	τ_3 (ps)	$\langle\tau_s\rangle^{fav}$ (ns)
0.0	235.4	0.35	14	0.34	114	0.31	769	0.29
0.2	140.6	0.32	19	0.34	85	0.34	714	0.27
0.4	90.4	0.39	14	0.35	125	0.27	625	0.21
0.6	64.2	0.53	15	0.25	98	0.22	575	0.16
0.8	49.0	0.40	6	0.30	83	0.30	400	0.15
1.0	38.6	0.17	11	0.55	73	0.28	294	0.12

[a] These numbers are better than ±10% of the reported values (estimated on the basis of limited data sets).

on our theoretical study that discusses the possible origins of the time scales observed in the present experiments.

It is already discussed that the Stokes' shift for a dipolar solute in these molten electrolyte solutions is determined mainly by the dipolar interaction between the solute and the dipolar host solvent molecules and ion−dipole interaction between the solute and the dissociated ions. However, the time scale of the Stokes' shift dynamics (or simply the solvation time scale) is governed by both the solute−medium interaction and the natural dynamics of the medium. Therefore, in addition to the solute−medium interactions, both the dipole−dipole interaction among the dipolar solvent molecules and ion−ion interaction among the dispersed ions contribute significantly to set the solvation time scales in these molten mixtures. Note that, in the above model, it is assumed that the arrangement of the dipolar solvent particles (both spatial and orientational) is not perturbed in the solution and the dynamics of the pure solvent is preserved. In addition, interaction between the ions and solvent molecules is not separately considered while calculating the Stokes' shift dynamics. This is an approximation as ion−solvent interaction can lead to modified solution properties that may or may not couple to the Stokes' shift dynamics in electrolyte solution. Ion−solvent interaction is also central to the *preferential solvation* of an ion[72,73] and the present model attempts neither to incorporate this effect on solvation of a dipolar solute nor to study the preferential solvation of the latter in such multicomponent mixtures. At the dynamic level, the effects of ion−solvent interaction are, however, partially incorporated through the use of experimental solution viscosity. Also note that the present theory expresses the measured Stokes' shift dynamics as a combination of separate contributions from "ion dynamics" and "dipolar solvent dynamics" where the "separability" between these two dynamical responses is based purely on the wide difference in the time scales of dynamic fluctuations of the ion and dipolar densities.[50,60] Even such a separation at the dynamic level is somewhat arbitrary as ion motion would entail solvent motion (and vice versa), but the fact that the solvent rotation being much faster than the ion translation provides some support to this approximation.[59,74]

In our first model study it is assumed that these molten mixtures respond to solute excitation via the *overdamped* dynamics where the environment rearranges through diffusion only.[75,76] Consequently, diffusive descriptions of both the solvent dynamic structure factor (eq 5 of the Appendix) and ion dynamic structure factor (eq 10 of the Appendix) are used in eq 13 of the Appendix for the calculation of the normalized total solvation response function ($S_E(t)$). The individual normalized response functions due to the solute−solvent dipole−dipole interaction ($S_{sd}(t)$) and solute−ion dipole−ion interaction ($S_{si}(t)$) have also been calculated by using respectively the eqs 14 and 15 of the Appendix in the *overdamped* limit of solvent response. Like the experimental $S(t)$'s, the theoretically calculated normalized solvation response functions have also been found to fit to triexponential functions of time. While the fit parameters for the calculated normalized response functions in the overdamped limit are summarized in Table 3a, the fit parameters for the individual response functions (S_{sd} and S_{si}) are presented in Table S4 of the Supporting Information. To facilitate comparison, the experimental average solvation times ($\langle\tau_s\rangle_{exp}$) are again tabulated in the last column of Table 3a. Representative triexponential fits to the calculated decays (S_{si} is considered as an example) have been shown in Figure S5 of the Supporting Information, revealing the quality of fits involved in these numerical descriptions of solvation response functions. Since in the overdamped limit the time scale is set by the viscosity of the medium alone, the time constants associated with each individual response functions shown in Table 3a are not very different from each other. Interestingly, except the longest time constant, which ranges between ∼1 and 5 ns, the other two calculated time constants are very similar to the experimentally obtained longer time constants (τ_2 and τ_3) given in Table 2. This suggests that these experimental time scales (τ_2 and τ_3) originate from the diffusive rearrangement of the environment surrounding the solute in these molten mixtures. The calculated longest time constant, which runs into several nanoseconds, has not been detected in the present experiments for these mixtures even though such a slow component for solvation dynamics in a few butylammonium ionic liquids near room temperature has been recently reported and explained in terms of longer-lived (relative to the excited state lifetime of the solute) local structure around the probe.[77] In the present theory, these nanosecond time constants arise due to slow diffusive relaxations of both the orientational *solvent* dynamic structure factor at the nearest neighbor ($k\sigma \rightarrow 2\pi$) modes[78] and translational *ion* dynamic structure factor involving the collective ($k\sigma \rightarrow 0$) modes.[66] It may therefore be stated that a slow component with a time constant ranging from a few to several nanoseconds is rather a *generic* property for solvent systems at or around the room temperature where ion−solute interaction makes a non-negligible contribution via slow ion translation to the total solvation energy relaxation. This is further supported by the fact that a time constant of a few nanoseconds has been observed for spectral evolutions even in electrolyte solutions of "fast" solvents at ∼296 K.[50] Lowering of solution temperature then further slows down the dynamics, lengthening the time constant dramatically. However, the respective contributions of $S_{sd}(t)$ and $S_{si}(t)$ to the total solvation energy relaxation ($S_E(t)$) determine the amplitudes of the components constituting the full decay and thus play a decisive role for the presence or absence of such an extremely slow component in the total solvation energy relaxation.

The next model study involves the calculation of the solute−solvent dipolar interaction contribution (S_{sd}) in the

TABLE 3: Triexponential Fit Parameters for the Calculated Solvation Response Functions at Various Mixture Compositions in the Overdamped Limit ($T \sim 318$ K)[a] and Biexponential Fit Parameters for the Calculated Solvation Response Functions in the Underdamped Limit at ∼318 K

(a) Triexponential Fit Parameters in the Overdamped Limit

f_{KSCN}	a_1	τ_1 (ps)	a_2	τ_2 (ps)	a_3	τ_3 (ps)	$\langle\tau_s\rangle$ (ns)	$\langle\tau_s\rangle_{exp}$ (ns)
0.0	0.07	90	0.85	580	0.08	4544	0.86	0.29
0.2	0.08	58	0.84	355	0.08	3141	0.55	0.27
0.4	0.09	38	0.84	233	0.07	2198	0.35	0.21
0.6	0.09	28	0.83	167	0.07	1632	0.25	0.16
0.8	0.10	23	0.83	131	0.07	1217	0.20	0.15
1.0	0.09	17	0.83	102	0.08	1016	0.17	0.12

(b) Biexponential Fit Parameters in the Underdamped Limit

f_{KSCN}	a_1	τ_1 (ps)	a_2	τ_2 (ps)	$\langle\tau_s\rangle$ (ns)
0.0	0.46	0.084	0.54	841	0.45
0.2	0.47	0.085	0.53	512	0.27
0.4	0.47	0.086	0.53	336	0.18
0.6	0.47	0.087	0.53	243	0.13
0.8	0.47	0.088	0.53	182	0.097
1.0	0.47	0.089	0.53	149	0.079

[a] Experimental average solvation times ($\langle\tau_s\rangle_{exp}$) are mentioned again in Table 3a to facilitate comparison with calculations.

underdamped limit of dipolar solvent (acetamide for these mixtures) dynamics.[39] In this limit where solvent frictional response includes the memory effects, proper calculations of the rotational and translational dissipative kernels are extremely important. Even though the calculation of the translational kernel is rather easy, the same for the rotational kernel is quite nontrivial. In the present study we use the calculation scheme elaborated in ref 39 (see also the Appendix) for obtaining the rotational kernel from the experimental dielectric relaxation data and translation memory kernel from the diffusive description of the isotropic solvent dynamic structure factor. However, one still faces a problem to calculate the rotational kernel for these molten mixtures as complete dielectric relaxation data are not available for these media. In the absence of any reliable and experimentally measured dielectric relaxation data for these systems, it is assumed that liquid acetamide in these molten mixtures would *qualitatively* follow the dispersion steps as observed in the dielectric relaxation of liquid formamide at room temperature.[81] In such a model where the rotation of an acetamide molecule is approximated as that of a spherical particle, the relaxation time is obtained from the Debye−Stokes−Einstein (DSE) relation by using the stick boundary condition. Following the dielectric relaxation data of formamide at room temperature,[81] the dispersion from $\varepsilon_0 \approx 30$ to $\varepsilon_1 \approx 5$ is attributed to the relaxation time calculated from the solution viscosity at each composition as described above. The remaining part, $\varepsilon_1 - n_D^2$, is then assumed to be carried out by the librational mode, which is often found to be centered around 100 cm^{-1} in amide systems.[68] These model dielectric relaxation data and other necessary parameters are summarized in Table S6 of the Supporting Information. Note that although the present scheme allows one to investigate the effects of librational mode on the early time dynamics of solvation response in these mixtures, the calculated solvation time constants may not be quite accurate because of the use of model dielectric relaxation data. This drawback notwithstanding, these calculations should be able to suggest qualitatively the fastest time constant associated with the solvation response in these molten mixtures. This assumes even more importance when one considers that dynamic Stokes' shift measurements presented here indicate missing almost half of the total shift due to a broad time resolution employed in experiments. The ion−dipole interaction part (S_{si}) has been calculated as before by assuming diffusive dynamics only, although calculations incorporating the inertial translational motions (of the ions) in the ion dynamic structure factor[79,80] did not produce any different results. This is because of the large translational friction (ζ_α^{ion} in the expression given in ref 79) experienced by the ions while moving through these highly viscous media.

The calculated solvation response functions due to the solute−solvent dipolar interaction (S_{sd}) in the limit of *underdamped* solvent dynamics have been found to be biexponential function of time at all compositions of the molten mixture studied here (see Table S7 in the Supporting Information). Fit parameters required to describe the calculated total solvation response function in this limit are summarized in Table 3b where one can find that a time constant of subhundred femtosecond component constitutes nearly 50% of the total calculated decay at all the mixture compositions. Note that the amplitude of this ultrafast component is surprisingly very similar to the missing portion of the total shift by our present measurements. In addition, the slowest time constant calculated in this limit is in qualitative agreement with both experimental data (τ_3 of Table 2) and those calculated in the overdamped limit (τ_2 of Table 3a). This is expected because the long-time dynamics is dominated by the diffusive motions of the solvating particles, and the present experiments have been able to detect mainly the slower part of the dynamics occurring relatively at the later stage of solvation in these systems. A very good agreement between the experimental and calculated average solvation times in these mixtures (last columns of Tables 2 and 3) is also a reflection of this fact as the average rate of solvation is dominated by the long-time constant.

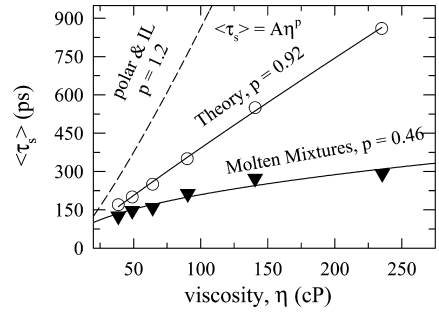

Figure 6. Medium viscosity (η) dependence of average solvation time, $\langle\tau_s\rangle$, for C153 in molten mixtures of acetamide with sodium and potassium thiocyanates. Triangles represent experiments, circles denote calculations in the overdamped limit and the broken line shows dependence in polar solvents and ionic liquids together. Note the later results are taken from ref 57 where the same solute (C153) has been used for experimental measurements. The η dependence of $\langle\tau_s\rangle$ in these media can be described by the following generic relation: $\langle\tau_s\rangle = A\eta^p$. The values of A (in proper unit) for these media are as follows: 3.43 for polar solvents and ionic liquids together, 5.5 for the overdamped calculations, and 25.36 for the molten mixtures. The respective values of the fraction (p) are indicated in the figure. The underdamped calculations (not shown here) produces 2.3 for A and 0.96 for p.

Average solvation times ($\langle\tau_s\rangle$) measured for these molten mixtures have been found to follow a fractional viscosity dependence ($\langle\tau_s\rangle \propto \eta^p$) with $p = 0.46$. A power law dependence of average solvation time on solvent viscosity with $p \sim 1$ is expected if simple diffusion regulates the solvation of a large solute probe at long time. In fact, a near proportionality between average solvation time and solvent viscosity (that is, $p \sim 1$) has been found when the relevant data in polar solvents and ionic liquids are considered together.[57] All these results are presented in Figure 6 where the viscosity dependence of the calculated average solvation time from overdamped dynamics are also shown for comparison. The pronounced fractional viscosity dependence ($p \sim 0.5$) of $\langle\tau_s\rangle$ in these mixtures is therefore distinctly different from what has been observed earlier in polar solvents and ionic liquids and indicates a much weaker coupling between the medium viscosity and translational motion of solvating particles. Fractional Stokes−Einstein (SE) behavior for particle diffusion ($D \propto \eta^{-p}$) is long-known for supercooled liquids near the glass transition and sometimes argued as diagnostic for dynamic heterogeneity of a given medium.[82−87] A significant departure from the SE relation is also expected for small solutes diffusing through a medium of large particles.[88] In addition, fractional SE behavior has been experimentally observed for a variety of systems, ranging from diffusion of inert solute at room temperature in water and aqueous mixtures[89,90] and ion transport in ionic melts[91] to temperature dependence of diffusion of atomic and molecular solutes in alkane solvents.[92−94]

Even though a number of alternative explanations have been proposed for the observed breakdown of SE relation in supercooled liquids and other viscous media,[95−98] a very recent work[99] suggests that the fractional SE relation holds as well for normal solvents, ionic liquids, and even self-diffusion in

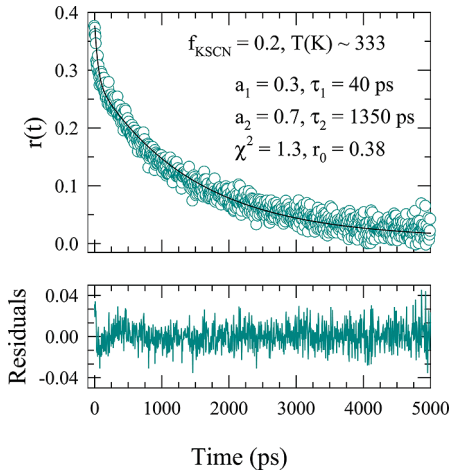

Figure 7. Representative fluorescence anisotropy decay, $r(t)$, of C153 at ~333 K in a molten mixture of acetamide with sodium and potassium thiocyanates with $f_{KSCN} = 0.20$. While circles represent experimental decay in the upper panel, the solid line denotes the fit. The fit parameters are shown in the inset. Bottom panel shows the residuals.

Lennard-Jones fluid in the liquid and dense supercritical states. However, except for diffusion of a few inert atomic solutes and methane in several nonaqueous solvents where the fraction is found to lie in the range $0.6 > p > 0.4$, other studies[82–87,89–91,99] have found p to vary approximately between 0.6 and 0.9. Therefore, the fractional power dependence on medium viscosity of average solvation time found in the present measurements is more similar to the diffusion−viscosity correlation observed for inert and small solutes in various solvents. This then raises the following question: is it the medium heterogeneity or the non-Fickian diffusion of relatively smaller alkali metal ions or even both responsible for the observed fractional power dependence? The diffusion of ions is relevant to the dynamic Stokes' shift since it is the ion−solvent exchange dynamics in the immediate neighborhood of the excited solute that contributes substantially to the spectral evolution in electrolyte solutions at longer times.[59] The medium heterogeneity can contribute to the solvation energy relaxation via the non-Gaussian dynamics of ions, such as, Levy flights.[100] A recent simulation study of ionic liquids have indeed revealed the presence of such dynamics where a certain percentage of ions are found to execute successive jumps that continued even much after the onset time of the diffusive motion.[101,102] Therefore, the hierarchical or multifractal dynamics of "fast" and "slow" ions found in simulations of ionic liquids may be one of the reasons for the observed decoupling of average solvation time from viscosity in these molten mixtures. The above argument, however, does not explain why the measured average solvation time in various ionic liquids exhibit a near proportionality to the medium viscosity. Further studies are thus required to completely understand the viscosity dependence of the solvation times in these complex mixtures.

C. Time-Resolved Fluorescence Anisotropy $r(t)$ and Its Temperature Dependence. Representative anisotropy decay of C153, constructed by using eq 2 from the collected parallel and perpendicular emission decays in one of these molten mixtures (at $f_{KSCN} = 0.2$) at ~333 K is shown in Figure 7. The biexponential fit through the data points (line) and the relevant fit parameters are also shown in the same figure. Following the anisotropy decay fits for C153 in several ionic liquids,[57,103] the value for the initial anisotropy (r_0) of C153 is fixed at 0.38 while fitting the anisotropy decays in these mixtures at all temperatures. The random nature of the residual (bottom panel) and the value of the *goodness of fit parameter* (χ^2) seems to suggest that a biexponential function of time reasonably describes the decay of $r(t)$ at this solution condition. In fact, considering the microscopic heterogeneity of these molten mixtures, fit to a stretched exponential function of the form $r(t) = r_0 \exp[-(t/\tau_{rot})^{\beta_{rot}}]$ was also attempted but produced worse fits than the biexponential descriptions. However, biexponential functions with a variation of ~10−15% in the amplitudes and time constants have been found to fit the decays equally well. Therefore, the error bar associated with these fit parameters is approximately ±10−15% of the reported values.

We briefly discuss here the overall results of anisotropy studies in ionic liquids since these liquids are somewhat linked (interaction-wise) to the molten mixtures under investigation. Both stretched and multiexponential functions have been found to fit the measured anisotropy decays with different dipolar solutes in a variety of ionic liquids.[77,103–107] The nonobservation of stretched exponential kinetics of $r(t)$ for C153 in these molten mixtures may originate from the following factors: (i) the broad time resolution used in the present experiments[108] and (ii) larger average lifetime of the probe compared to the trapping time of the solute in the spatially heterogeneous quasistatic local solvent environments.[28,31,109,110] Although the excitation wavelength (λ_{exc}) dependence of the solute anisotropy in these molten mixtures is yet to be explored, our initial investigation reveals that for moving the λ_{exc} from 360 to 490 nm across the absorption band of C153 in this mixture at $f = 0.2$ and ~318 K, the observed shift (total) in the solute's emission peak frequency (steady state) is only ~400 cm^{-1} with the accompanying total change in full-width-at-half-maximum of ~140 cm^{-1} (see Figure S8, Supporting Information). These results, when juxtaposed with the already observed near constancy of the width of the time-resolved emission spectrum in these molten mixtures, partially explain why stretched exponential kinetics for $r(t)$ have not been observed in the present systems. Since multiexponential kinetics have also been observed in single component viscous liquids ("slow" solvents)[60] at ambient condition, it is conjectured that the non-Markovian nature of the rotational friction rather than the spatial heterogeneity in the environment gives rise to the multiexponential anisotropy decays in ionic liquids.[103,104] This can also be the reason for the observed biphasic nature of $r(t)$ in the present mixtures, but the heterogeneity effects may also be responsible for the observed deviation from the exponential decay kinetics. Therefore, a more extensive study, probably with solute probes of differing excited state average lifetimes,[28] is required to fully explore the heterogeneity (spatial and temporal) and its effects on various relaxation processes in these molten mixtures.

The decay parameters shown in Figure 7 suggest that the average rotation time ($\langle\tau_r\rangle$) of C153 in this mixture at 333 K is nearly a nanosecond ($\langle\tau_r\rangle$ = 957 ps). Now if one uses the *modified* Debye−Stokes−Einstein (DSE) relation, $\tau^{(2)} = (V\eta/k_BT)fC$, with solute volume $V = 246$ Å^3 and shape factor $f = 1.71$, then the slip boundary conditions ($C = 0.24$)[104] predict an average rotation time of ~2 ns for C153 in this mixture at this temperature ($\eta \approx 50$ cP).[44] The same DSE relation with stick boundary conditions ($C = 1$), on the other hand, estimates the $\langle\tau_r\rangle$ as ~8 ns. What is revealed by these calculations is that even though the DSE relation, with proper solute shape factor and boundary condition, correctly predicts the right order of magnitude for $\langle\tau_r\rangle$, the absolute magnitude is considerably different from what has been observed in these experiments. This is probably an indication of partial decoupling of solute rotation from the medium viscosity and is reminiscent of what has already been observed in supercooled liquids.[82] To explore

TABLE 4: Parameters Obtained from Biexponential Fits to $r(t)$ of C153 in a Molten Mixture of Acetamide with Sodium and Potassium Thiocyanates at Various Mixture Compositions and Temperatures[a]

f_{KSCN}	T (K)	viscosity (cP)	a_1	a_2	τ_1 (ps)	τ_2 (ps)	$\langle\tau_r\rangle$ (ps)
0.0	318	235.4	33.96	66.04	29	4021	2665
0.2	318	140.6	34.23	65.77	29	3192	2109
0.4	318	90.4	33.20	66.80	38	2419	1629
0.6	318	64.2	31.19	68.81	22	1994	1379
0.8	318	49.0	29.00	71.00	17	1640	1170
1.0	318	38.6	29.48	70.52	42	1462	1044
0.2	333	52.6	36.29	63.71	41	1480	958
	348	29.0	39.33	60.67	49	859	541
	363	(13.4)	37.13	62.87	27	447	291
	373	(8.00)	43.82	56.18	39	342	209
0.8	333	23.0	32.29	67.71	40	877	607
	348	15.0	40.09	59.91	47	527	335
	363	(6.98)	38.37	61.63	37	331	218
	373	(4.55)	47.85	52.15	42	277	164

[a] Values in parentheses have been obtained from extrapolating the viscosity data provided in ref 44. a_1 and a_2 are in percentage.

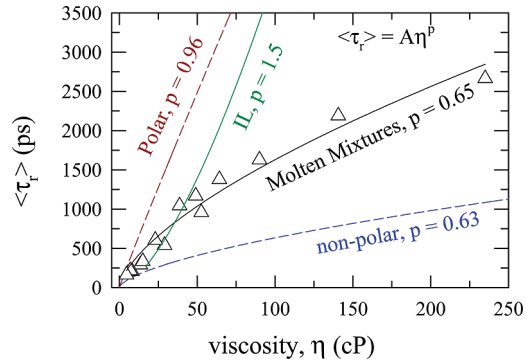

Figure 8. Viscosity dependence of average rotational time for C153, $\langle\tau_r\rangle$, in molten mixtures of acetamide with sodium and potassium thiocyanates. While the triangles represent data from present experiments, the solid green line denotes dependence for ionic liquids, dashed red lines for polar solvents, and dashed blue lines for nonpolar solvents. Correlations for C153 in polar and nonpolar solvents have been taken from ref 60, and for ionic liquids, the correlation is generated by using data presented in ref 104. For rotation also, the viscosity dependence can be expressed as follows: $\langle\tau_r\rangle = A\eta^p$. The values of p for different media are indicated in the figure itself. A values are (in proper unit): 58.1 (polar solvents), 3.7 (ionic liquids), 80.6 (molten mixtures), and 34.8 (nonpolar solvents).

further the relationship between the viscosity and solute rotation, we have followed the temperature dependence of solute rotation at two different fractions of KSCN (f_{KSCN} = 0.2 and 0.8). For these two molten mixtures, the anisotropy study has been carried out at five different temperatures at which viscosity values of the respective mixtures are already known.[44] Parameters obtained from biexponential fits to the anisotropy decays at these KSCN concentrations and temperatures are provided in Table 4 while the representative decays of $r(t)$ at three different temperatures at f_{KSCN} = 0.8 are presented in the Supporting Information (Figure S9). The correlations between $\langle\tau_r\rangle$ and η obtained from these measurements as well as those observed with the same solute in common dipolar and nonpolar solvents[60] and ionic liquids[104] are shown in Figure 8. A comparison among these results clearly indicate that even though the average rotation time in all these liquids exhibits a power-law dependence on viscosity (that is, $\langle\tau_r\rangle \propto \eta^p$), the dependence in molten mixtures is showing a *fractional* DSE behavior with p = 0.65. Surprisingly, the fractional power dependence of $\langle\tau_r\rangle$ on η is very similar to that found in nonpolar solvents (p = 0.63) and is somewhat *counterintuitive* in the sense that solute rotation in these mixtures is expected to be much closer to that in ionic liquids rather than in homogeneous nonpolar solvents where solute−solvent interaction is relatively much weaker.

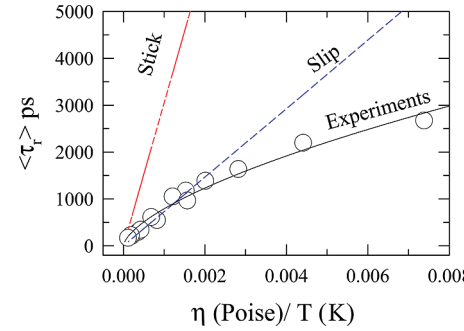

Figure 9. Prediction of stick (red dotted line) and slip (blue dotted line) hydrodynamics for solute rotation in these molten mixtures and comparison with experimental data (circles). The line going through the circles is a fit to the relation: $\langle\tau_r\rangle = A(\eta/T)^{0.64}$ with A (proper unit) = 64832 and R (correlation coefficient) = 0.98.

It is interesting to note that a crossover from the conventional DSE behavior to fractional DSE type viscosity dependence for rotation time has been reported[111–121] in a number of systems at temperatures broadly located around $1.2T_g$. All these studies have shown a considerable degree of decoupling ($0.25 \le p \le 0.75$) between the solute rotation and medium viscosity, and this phenomenon is attributed to the heterogeneous dynamics of the media investigated. Interestingly, model calculations based on the presence of dynamic heterogeneities have predicted fractional DSE behavior for a solute guest with the fraction (p) ranging from 0.25 to 0.7 depending upon the number of solvent (guest) molecules required to rearrange during the process of solute rotation.[113] If we now recall that the T_g of a binary mixture of acetamide with 0.225 mol fraction of sodium thiocyanate is ~230 K,[24,25] and the melting temperature of acetamide is ~350 K, then these present ternary mixtures may be considered as supercooled liquids where the observed deviation from the conventional hydrodynamic behavior may be attributed to both the spatial and temporal heterogeneities of these molten mixtures. In addition, the obstruction model for translational motion in glass-forming liquids has predicted a fractional viscosity dependence with p = 0.6.[122] This is surprisingly close to that found in the correlation between the average solvation time and viscosity in these molten mixtures. Further investigation involving these molten mixtures is therefore required to ascertain how much of the decoupling between $\langle\tau_s\rangle$ and η originates from the non-Gaussian dynamics of the solvent particles, and to what extent the observed fractional DSE behavior for $\langle\tau_r\rangle$ is dictated by the microscopic heterogeneity of these molten mixtures and the anisotropic diffusion around the individual molecular axes of the solute probe.[54,123–125]

Next we explore the usefulness of the conventional hydrodynamic relations for describing the solute rotation in these complex molten mixtures. The results are summarized in Figure 9 where the average rotation times obtained from the temperature dependent study of these mixtures at KSCN fractions 0.2 and 0.8 are shown as a function of η/T. The DSE predictions at slip and stick boundary conditions for an ellipsoidal rotor have been obtained by using the necessary parameters discussed already in the text and also presented in the same figure for comparison (solid lines). These results clearly indicate for solute rotation a transition from *slip* behavior at high temperature and low viscosity regime to *subslip* dependence at high viscosity and low temperature. The observed nonconformity to the proportionality to η/T is rather interesting given the fact that

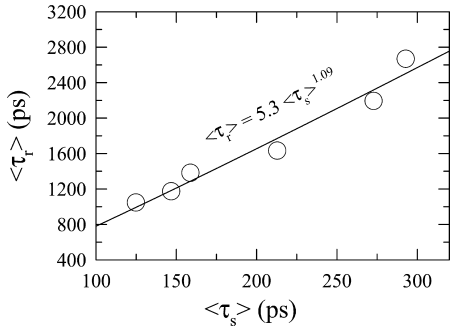

Figure 10. Experimental average rotational correlation times ($\langle\tau_r\rangle$) versus solvation times ($\langle\tau_s\rangle$) for C153 in these molten mixtures at $T \sim 318$ K. $\langle\tau_s\rangle$ at higher temperatures could not be obtained because of the broader temporal resolution employed in the present experiments. The line going through the circles represents a fit to the relation shown in the panel. A close examination of solvation and rotation data for most of the ionic liquids (except the phosphonium ones) summarized in ref 57 also indicate such a proportionality: $\langle\tau_r\rangle = 9.33\langle\tau_s\rangle^{1.03}$.

rotation times in ionic liquids follow essentially the same correlation as established in common dipolar solvents.[57] The deviation from the DSE prediction is, however, nothing new as fluorescence anisotropy studies with C153 and other solutes in normal alkane solvents[60,126,127] have already revealed such a fractional coupling between solute rotation and solvent viscosity. In alkane solvents, the solute−solvent coupling parameter (C in DSE) has been found to decrease with the increase in alkyl chain length due to inefficient solvent packing around the rotating solute.[60] In these molten mixtures, such a change in solute−solvent coupling may arise from distribution of solutes in different domains at low temperature and high viscosity conditions. Given the results that rotation of relatively larger solutes averages out environmental fluctuation more effectively than translation,[128,129] and the observation of negligible λ_{exc} dependence of the solute emission spectrum in these molten mixtures, it is not clear at the present moment how much of the fractional viscosity dependence arises from the medium heterogeneity and to what extent the interaction between the solute and polymerized (cation-induced) acetamide[22−25] (and thus less packing as in the case of alkanes) contributes to the breakdown of the conventional DSE law in these media.

Since both average solvation and rotation times are dictated substantially by the fluidity of the medium and since both of these quantities exhibit fractional viscosity dependence in these molten mixtures, it may be interesting to explore whether these times, like in ionic liquids,[130] maintain a linear relationship between them in these media. Results shown in Figure 10 clearly reveal such a relationship where the dependence can be expressed as follows: $\langle\tau_r\rangle = 5.26\langle\tau_s\rangle^{1.09}$, with a correlation coefficient (R) of 0.99. Note that these data correspond to the ternary mixture with different f_{KSCN}, but at a fixed temperature (318 K). Even though the above parametrization is based upon a rather limited set of data, a more extensive study (consideration of other KSCN fractions and different temperatures) is not expected to change the above relation significantly.[131] In addition, the present results are in conformity with the measurements of probe solvation and rotation in organic glass-forming liquids near T_g with several probes where average rotation times have been found to be always larger than the solvation times.[132] Interestingly, the fact that $\langle\tau_r\rangle$ is approximately 5 times larger than $\langle\tau_s\rangle$ in these molten mixtures is approximately in midway between what has been observed for rotation and solvation of C153 in alkylphosphonium ionic liquids (a factor of ∼2−3) and imidazolium ionic liquids (a factor of ∼8−10).[103] This similarity with ionic liquids together with the fact that the greater degree of decoupling from solvent viscosity for $\langle\tau_s\rangle$ ($p = 0.46$) than for $\langle\tau_r\rangle$ ($p = 0.65$) constructs a kinship to supercooled liquids where studies near T_g have shown stronger coupling between structural relaxation and rotation than between the former and translation.[98]

IV. Conclusion

The fluorescence spectroscopic study of molten mixtures of acetamide with sodium and potassium thiocyanates has generated several interesting results. Most important is the observation of fractional power law dependence on solution viscosity of both average solvation and rotational times for a dipolar solute in these molten multicomponent mixtures. Curiously, the degree of decoupling from solution viscosity for average solvation is similar to the small molecule translation in ambient liquids and, for rotation, to the breakdown of DSE law in supercooled liquids near to T_g. In addition, the translational decoupling (via average solvation time) has been found to be stronger than that in the case of solute rotation—a result that resembles qualitatively the findings in supercooled liquids. A transition from slip to subslip behavior for solute rotation in these molten mixtures has been found as the temperature-scaled viscosity is increased. The role of multifractal dynamics in light of the very recent computer simulation study of ionic liquids[101] and effects of solution heterogeneity have been discussed in connection with the observed breakdown of conventional hydrodynamic relations for translation and rotation in these molten systems.

The observed nonmonotonic alkali metal ion concentration dependence of both steady state and dynamic fluorescence Stokes' shifts have been explained in terms of solute−solvent and solvent−solvent interaction and medium heterogeneity due to presence of dissimilar cations and ion-induced solvent polymerization.[15] The nonmonotonic dependence is qualitatively similar to the results obtained by various physicochemical measurements done earlier for these mixtures and often explained in terms of mixed alkali effects. Even though solution heterogeneity has been found to play a greater role in explaining the viscoelastic, dielectric relaxation, and other experimental results of these and similar systems, the present study finds no or a secondary role of microscopic inhomogeneity of solution structure on fluorescence shifts or spectral evolution. Of course, it is to be remembered that the present experiments have missed almost half of the total dynamics due to limited time resolution and the nonfinding of the heterogeneity effects could be linked to this inability of fast detection.

Further studies should be done in the future with these molten systems to understand the extent of heterogeneity and its effects on dynamical events occurring in them. Neutron scattering and X-ray diffraction experiments may be carried out to ascertain the heterogeneity and the length scale associated with it in these complex ternary mixtures. Dielectric relaxation study with wider frequency coverage should be employed to study more carefully the low frequency as well as high frequency relaxation processes. The high frequency dielectric relaxation results could then be complimented by Kerr spectroscopic studies and understand further the intermolecular vibrational dynamics in these nonaqueous electrolyte solutions at elevated temperature.[133,134] This is particularly important as the dielectric relaxation data constitute a crucially important input for the kind of theory used here to predict the solvation time scales in these molten mixtures. Since calculations presented here seem to suggest the existence of an ultrafast time scale in the subpicosecond range, dynamic Stokes' shift measurements with better time resolution would be helpful in uncovering the entire dynamics of these systems as well as the predictive power

of the theory employed here. The heterogeneity effects can be further studied by using other solvatochromic probes possessing shorter average excited state lifetimes than the one used here. Computer simulations with proper treatment of the longer-ranged ion−dipole and dipole−dipole interactions can significantly help understand results from many of the proposed experiments. Since dynamical studies of these molten mixtures with sophisticated time and space resolutions have not been done yet, these systems can offer interesting possibilities and results that can stimulate scientists for quite some time.

Acknowledgment. We thank Dr. S. Mahiuddin, NEIST, Jorehat, for drawing our attention to some of his works in this field and Mr. Biman Jana, a graduate student in the research group of Professor B. Bagchi, IISc., Bangalore for helping us access several important references. We are thankful to Professors M. Maroncelli and R. Buchner for many helpful comments. B.G. thanks CSIR for a research fellowship. H.G. expresses his sincere thanks to the Vice-Chancellor, Aliah University, West Bengal, for encouragement.

Supporting Information Available: Figures containing KSCN concentration dependent viscosity and longest time constant ($\tau_{Longest}$) obtained from magic angle fluorescence intensity decays, fits to calculated solvation response functions, excitation wavelength dependence of fluorescence emission peak frequency, and temperature dependence of anisotropy decays at a given mixture composition. Tables containing experimental density of the mixtures studied, model dielectric relaxation data, and other parameters necessary for the theoretical calculations of solvation response function. This material is available free of charge via the Internet at http://pubs.acs.org.

Appendix: Theoretical Formulation and Calculation Details

In this section we shall present the necessary expressions for calculating the total solvation response functions for a dipolar solute dissolved in the molten mixtures of acetamide with sodium and potassium thiocyanates. The starting point here is again the classical density functional theory where the total excess free energy functional for these electrolyte solutions can be written as a function of dipolar solute dissolved in a medium consisting of dipoles and ions.[39] In equilibrium, the derivative of this excess free energy with respect to the solute density is zero (because of free energy minimum) and this condition provides the average solvation energy for solute due to its interaction with the neighboring dipoles and ions. For derivation, kindly see the Supporting Information of ref 66a. The expression for the position ($\mathbf{r}$), orientation ($\mathbf{\Omega}$), and time (t) dependent solvation energy for mobile dipolar solute with distribution function $\rho_s(\mathbf{r},\mathbf{\Omega};t)$ can then be written as follows[66a]

$$\Delta E_{total}(\mathbf{r},\mathbf{\Omega};t) = -k_B T \rho_s(\mathbf{r},\mathbf{\Omega};t)\Big[\int d\mathbf{r}'\, d\mathbf{\Omega}'\, c_{sd}(\mathbf{r},\mathbf{\Omega};\mathbf{r}',\mathbf{\Omega}')\, \delta\rho_d(\mathbf{r}',\mathbf{\Omega}';t) + \sum_{\alpha=1}^{2} \int d\mathbf{r}'\, c_{s\alpha}(\mathbf{r},\mathbf{\Omega};\mathbf{r}')\, \delta n_\alpha(\mathbf{r}';t)\Big] \quad (1a)$$

$$= \Delta E_{sd}(\mathbf{r},\mathbf{\Omega};t) + \Delta E_{si}(\mathbf{r},\mathbf{\Omega};t)$$

$c_{sd}(\mathbf{r},\mathbf{\Omega};\mathbf{r}',\mathbf{\Omega}')$ and $c_{s\alpha}(\mathbf{r},\mathbf{\Omega};\mathbf{r}')$ are respectively the position and orientation dependent solute dipole−solvent dipole (dipole−dipole) and solute dipole−ion (dipole−ion) direct correlation functions and α denotes the type of ions (cation and anion). The fluctuations in dipolar density ($\delta\rho_d$) and ion density (δn_α) from the respective bulk values are defined as follows: $\delta\rho_d(\mathbf{r},\mathbf{\Omega}) = \rho_d(\mathbf{r},\mathbf{\Omega}) - \rho_d^0/4\pi$ and $\delta n_\alpha(\mathbf{r}) = n_\alpha(\mathbf{r}) - n_\alpha^0$. Therefore, the solvation energy−energy correlation function averaged over space ($\mathbf{r}$) and orientation ($\mathbf{\Omega}$) for such system is written as[66a]

$$C_E(t) = C_{sd}(t) + C_{si}(t) \quad (2a)$$

where $C_{sd}(t)$ and $C_{si}(t)$ are the energy−energy correlation functions for dipole−dipole and dipole−ion interactions, respectively. Note that in writing down eq 2a one assumes that cross-correlation between fluctuating energies vanishes due to very different time scales involved in fluctuations of dipolar solvent and ion densities.[66a] As already mentioned, this may not be true as ion and solvent translational motions are likely to be coupled and, consequently, will be relevant for the intermediate to long-time dynamics.

The expressions for $C_{sd}(t)$ and $C_{si}(t)$ are given by[66a]

$$C_{sd}(t) = \langle \Delta E_{sd}(t)\, \Delta E_{sd}(0)\rangle = 2\rho_d^0\left(\frac{k_B T}{2\pi}\right)^2 \Big[\int_0^\infty dk\, k^2 S^{10}_{solute}(k;t)|c^{10}_{sd}(k)|^2 S^{10}_{solvent}(k;t) + 2\int_0^\infty dk\, k^2 S^{11}_{solute}(k;t)|c^{11}_{sd}(k)|^2 S^{11}_{solvent}(k;t)\Big] \quad (3a)$$

and

$$C_{si}(t) = \langle \Delta E_{si}(t)\, \Delta E_{si}(0)\rangle = 2\left(\frac{k_B T}{2\pi}\right)^2 \sum_{\alpha,\beta} \sqrt{n_\alpha^0 n_\beta^0} \int_0^\infty dk\, k^2 S^{10}_{solute}(k;t) \times c^{10}_{s\alpha}(k)\, c^{10}_{s\beta}(-k)\, S^{ion}_{\alpha\beta}(k;t) \quad (4)$$

In the above expressions $c^{lm}_{sd}(k)$ represents the Fourier transform of the (l, m) component of the static direct correlation function between the solute and dipolar species, and $S^{lm}_{solvent}(k,t)$ is the same component of the orientational dynamic structure factor of the dipolar species. The expression for $S^{lm}_{solvent}(k,t)$ in the diffusive limit can be written as[75,76]

$$S^{lm}_{solvent}(k,t) = S^{lm}_{solvent}(k)\exp\left[-(l(l+1)D_R + k^2 D_T)\left(1 - \frac{\rho_d^0}{4\pi} c^{llm}(k)\right)\right] \quad (5)$$

where $S^{lm}_{solvent}(k)$, the orientational static structure factor for the dipolar solvent, can be calculated from the mean spherical approximation (MSA). D_R and D_T are the rotational and translational diffusion coefficients of the dipolar molecule and are calculated from the medium viscosity by using the stick boundary condition. $c^{llm}(k)$ is the (l, m) component of direct correlation function for the dipolar solvent, which can also be obtained by using the MSA. $S^{lm}_{solute}(k,t)$ denotes the (l, m) component of the solute self-dynamic structure factor which, in the diffusive limit, is approximated as

$$S^{lm}_{\text{solute}}(k,t) = \frac{1}{4\pi}\exp[-(l(l+1)D^{s}_{R} + k^2 D^{s}_{T})t] \quad (6)$$

The rotational (D^{s}_{R}) and translational (D^{s}_{T}) diffusion coefficients of the solute are obtained from the solution viscosity by using respectively the stick and slip boundary conditions. The longitudinal component of the wavenumber dependent direct correlation function between the dipolar solute and ions, $c^{10}_{s\alpha}(k)$ is taken as[66a]

$$c^{10}_{s\alpha}(k) = -\sqrt{\frac{4\pi}{3}}\left(\frac{4\pi i \mu_1 q_\alpha}{k_B T \varepsilon_0 k}\right)\frac{\sin(kr_c)}{kr_c} \quad (7)$$

where μ_1 is the dipole-moment of the dipolar solute, q_α is the charge of αth type ion, ε_0 is the static dielectric constant, and r_c is the distance of the closest approach between the solute dipole and the ionic species. $S^{ion}_{\alpha\beta}(k,t)$ denotes the isotropic ion dynamic structure factors. We have assumed each of the ions as singly charged hard spheres with equal radii and used the expressions derived elsewhere for the calculation of ion static structure factor, $S^{ion}_{\alpha\beta}(k)$. Using the aforementioned assumption, eq 4 can be further simplified as[135,136]

$$C_{si}(t) = 2\left(\frac{k_B T}{2\pi}\right)^2 \int_0^\infty dk\, k^2 S^{10}_{\text{solute}}(k;t)\, c^{10}_{s}(k)\, c^{10}_{s}(-k) \times \sum_{\alpha,\beta}\sqrt{n^0_\alpha n^0_\beta}\, q_\alpha q_\beta S^{ion}_{\alpha\beta}(k;t) \quad (8)$$

or

$$C_{si}(t) = 2\left(\frac{k_B T}{2\pi}\right)^2 \int_0^\infty dk\, k^2 S^{10}_{\text{solute}}(k;t)\, c^{10}_{s}(k)\, c^{10}_{s}(-k) L^{-1} \times \left(\sum_{\alpha,\beta}\sqrt{n^0_\alpha n^0_\beta}\, q_\alpha q_\beta S^{ion}_{\alpha\beta}(k;z)\right) \quad (9)$$

and

$$c^{10}_{s}(k) = \frac{c^{10}_{s\alpha}(k)}{q_\alpha},$$

where L^{-1} stands for Laplace inversion from the frequency (z) plane to the time (t) plane, and

$$\sum_{\alpha,\beta}\sqrt{n^0_\alpha n^0_\beta}\, q_\alpha q_\beta S^{ion}_{\alpha\beta}(k;z) = \frac{1}{Z(k,z)}[z\sum_{\alpha,\beta}\sqrt{n^0_\alpha n^0_\beta}\, q_\alpha q_\beta S^{ion}_{\alpha\beta}(k) + D^{ion}_2 k^2 \Delta(k)\{\sqrt{n^0_1}\, q_1 S^{ion}_{11}(k) + \sqrt{n^0_2}\, q_2 S^{ion}_{12}(k)\}^2 + D^{ion}_1 k^2 \Delta(k)\{\sqrt{n^0_2}\, q_2 S^{ion}_{22}(k) + \sqrt{n^0_1}\, q_1 S^{ion}_{21}(k)\}^2] \quad (10)$$

where

$$Z(k,z) = z^2 + z\Delta(k)[D^{ion}_1 k^2 S^{ion}_{22}(k) + D^{ion}_2 k^2 S^{ion}_{11}(k)] + D^{ion}_1 D^{ion}_2 k^4 \Delta(k) \quad (11)$$

and

$$\Delta(k) = [S^{ion}_{11}(k)\, S^{ion}_{22}(k) - S^{ion}_{12}(k)^2]^{-1} \quad (12)$$

Note that $S^{ion}_{\alpha\beta}(k)$ (with $\alpha, \beta = 1$ or 2) can be approximated by the Percus−Yevick (P−Y) solution of binary hard-sphere mixture.[137] We have assumed each of the ions as singly charged hard spheres with equal radii and used the expressions derived elsewhere[135,136] for the calculation of partial ion static structure factor, $S^{ion}_{\alpha\beta}(k)$.

Finally, eq 2a is normalized to give following expression for normalized solvation response function as

$$S_E(t) = \frac{C_{sd}(t=0)^2}{[C_{sd}(t=0)^2 + C_{si}(t=0)^2]} S_{sd}(t) + \frac{C_{si}(t=0)^2}{[C_{sd}(t=0)^2 + C_{si}(t=0)^2]} S_{si}(t) \quad (13)$$

where the contribution due to the solute−solvent dipolar interaction is given as

$$S_{sd}(t) = \frac{C_{sd}(t)\, C_{sd}(t=0)}{C_{sd}(t=0)^2} \quad (14)$$

and that due to the solute−ion (dipole−ion) interaction can be expressed as

$$S_{si}(t) = \frac{C_{si}(t)\, C_{si}(t=0)}{C_{si}(t=0)^2} \quad (15)$$

Note that the individual response functions given by eqs 14 and 15 are normalized ones and the present theory predicts that the total solvation response function measured in experiments derives contributions from both of these individual components. Note also that following the arguments provided in ref 66a, the dipole−dipole and ion−dipole contribution to dynamic Stokes' shift have been calculated respectively from the square root of the denominators of eq 14 and eq 15.

However, calculation of the total solvation response function in the *underdamped* limit by using eq 13 requires the proper calculation of $S^{lm}_{\text{solvent}}(k,t)$. This is composed of longitudinal (10) and transverse (11) components of the orientational solvent dynamic structure factors which have been shown to be given by[39−41]

$$S^{10}_{\text{solvent}}(k,t) = \frac{1}{4\pi 3Y}\left[1 - \frac{1}{\varepsilon_L(k)}\right]L^{-1}\{z + \sum_{10}(k,z)\}^{-1} \quad (16)$$

and

$$S^{11}_{\text{solvent}}(k,t) = \frac{1}{4\pi 3Y}[\varepsilon_T(k) - 1]L^{-1}\{z + \sum_{11}(k,z)\}^{-1} \quad (17)$$

where 3Y is the polarity parameter of the dipolar solvent obtained from the solvent dipole−moment and density (ρ^0_d) as $3Y = (4\pi/3k_BT)\mu^2\rho^0_d$. $\varepsilon_L(k)$ and $\varepsilon_T(k)$ are the longitudinal and transverse components of the wavenumber dependent dielectric function, respectively. $\Sigma_{lm}(k,z)$ denotes the (l, m)th component of the generalized rate of orientational solvent polarization density relaxation of the pure dipolar solvent. The calculation

of $\Sigma_{lm}(k,z)$ is rather complex. It is determined by the static orientational structure, frequency dependent dielectric function $\varepsilon(z)$, and translational diffusion coefficient of the solvent molecule. The expression for the generalized rate of orientational polarization density relaxation is given by[39–42]

$$\sum_{lm}(k,z) = \frac{k_B T k^2 f(llm,k)}{M\sigma^2[z + \Gamma_T(k,z)]} + \frac{k_B T l(l+1) f(llm,k)}{I[z + \Gamma_R(k,z)]} \tag{18}$$

where σ, M, and I are the diameter, mass, and average moment of inertia of the solvent molecule, respectively. $\Gamma_T(k,z)$ and $\Gamma_R(k,z)$ are the wavenumber and frequency dependent translational and rotational memory kernels, respectively. $f(llm,k) = 1 - (\rho_d^0/4\pi)(-1)^m c(llm,k)$, describes the (1, 1, 0), (1, 1, 1), and (1, 1, −1) components of the orientational static structure of the dipolar solvent. $\varepsilon_L(k)$ and $\varepsilon_T(k)$ are connected to $f(llm,k)$ by the following relations,[39] $[1 - (1/\varepsilon_L(k))] = 3Y/f(110,k)$ and $[\varepsilon_T(k) - 1] = 3Y/f(111,k)$. Subsequently, the mean spherical approximation (MSA) has been used to compute $f(llm,k)$ from the wavenumber dependent orientational direct correlation function, $c(llm,k)$ with proper corrections[39] at both $k\sigma \rightarrow 0$ and $k\sigma \rightarrow \infty$ limits.

Of these two frictional memory kernels, the calculation of $\Gamma_T(k,z)$ is somewhat easier and has been obtained from the isotropic liquid dynamic structure factor, $S(k,z)$, using the relation[39]

$$\frac{k_B T}{M\sigma^2[z + \Gamma_T(k,z)]} = \frac{S(k)[S(k) - zS(k,z)]}{k^2 S(k,z)} \quad \text{with}$$
$$S(k,z) = \frac{S(k)}{z + D_T k^2/S(k)} \tag{19}$$

The rotational memory kernel $\Gamma_R(k,z)$ has been obtained by using the frequency dependent dielectric function $\varepsilon(z)$ as follows[39]

$$\frac{2k_B T}{I[z + \Gamma_R(k,z)]} = \frac{z\varepsilon_0[\varepsilon(z) - \varepsilon_\infty]}{f(110;k=0)\,\varepsilon_\infty[\varepsilon_0 - \varepsilon(z)]} \tag{20}$$

where ε_0 is the static dielectric constant of the medium and ε_∞ is $\varepsilon(z)$ in the high frequency limit. $\Sigma_{11}(k,z)$ can be obtained in a similar manner from the experimental dielectric relaxation data by using eq 20 and multiplying it with $f(111,k)$.

References and Notes

(1) Stafford, O. F. *J. Am. Chem. Soc.* **1933**, *55*, 3987.
(2) Yntema, L. F.; Audrieth, L. F. *J. Am. Chem. Soc.* **1930**, *52*, 2693.
(3) Dawson, L. R.; Sears, P. G.; Graves, R. H. *J. Am. Chem. Soc.* **1955**, *77*, 1986.
(4) Wallace, R. A. *Inorg. Chem.* **1972**, *11*, 414.
(5) Wallace, R. *J. Phys. Chem.* **1971**, *75*, 2687.
(6) Jander, G.; Winkler, G. *J. Inorg. Nucl. Chem.* **1959**, *9*, 24.
(7) Wallace, R.; Bruins, P. *J. Electrochem. Soc.* **1967**, *114*, 212.
(8) Dev, S.; Das, D.; Ismail, K. *J. Chem. Eng. Data* **2004**, *49*, 339.
(9) Dev, S.; Ismail, K. *J. Chem. Eng. Data* **2001**, *46*, 574.
(10) Kalita, G.; Sarma, K. G.; Mahiuddin, S. *J. Chem. Eng. Data* **1999**, *44*, 222.
(11) Dev, S.; Gunaseelan, K.; Ismail, K. *Langmuir* **2000**, *16*, 6110.
(12) Akhter, M. S. *Colloids Surf. A* **1995**, *99*, 255.
(13) Akhter, M. S.; Alawi, S. M.; Bose, A. N. *Colloids Surf. A* **1995**, *94*, 173.
(14) Gusteri, M.; Bartocci, V.; Castellani, F.; Pucciarelli, F. *J. Electroanal. Chem.* **1979**, *102*, 199.
(15) (a) Castellani, F.; Berchiesi, G.; Pucciarelli, F.; Bartocci, V. *J. Chem. Eng. Data* **1981**, *26*, 150. (b) Berchiesi, G.; Angelis, M. D.; Rafaiani, G.; Vitali, G. *J. Mol. Liq.* **1992**, *51*, 11.
(16) Castellani, F.; Berchiesi, G.; Pucciarelli, F.; Bartocci, V. *J. Chem. Eng. Data* **1982**, *27*, 45.
(17) Berchiesi, G.; Lobbia, G. G.; Bartocci, V.; Vitali, G. *Thermochim. Acta* **1983**, *70*, 317.
(18) Lobbia, G. G.; Berchiesi, G.; Poeti, G. *Thermochim. Acta* **1984**, *74*, 247.
(19) Berchiesi, G.; Lobbia, G. G.; Berchiesi, M. A.; Vitali, G. *J. Therm. Anal.* **1984**, *29*, 729.
(20) Lobbia, G. G.; Berchiesi, G. *Thermochim. Acta* **1984**, *74*, 251.
(21) Lobbia, G. G.; Berchiesi, G. *Thermochim. Acta* **1984**, *72*, 391.
(22) Berchiesi, G.; Rafaiani, G.; Vitali, G.; Farhat, F. *J. Therm. Anal.* **1995**, *44*, 1313.
(23) Berchiesi, G.; Vitali, G.; Passamonti, P.; Plowiec, R. *J. Chem. Soc., Faraday Trans. 2* **1983**, *79*, 1257.
(24) Amico, A.; Berchiesi, G.; Cametti, C.; Biasio, A. D. *J. Chem. Soc., Faraday Trans. 2* **1987**, *83*, 619.
(25) Berchiesi, G. *J. Mol. Liq.* **1999**, *83*, 271.
(26) Wang, Y.; Voth, G. A. *J. Am. Chem. Soc.* **2005**, *127*, 12192.
(27) Triolo, A.; Russina, O.; Bleif, H.; Cola, E. D. *J. Phys. Chem. B* **2007**, *111*, 4641.
(28) Mandal, P. K.; Sarkar, M.; Samanta, A. *J. Phys. Chem. A* **2004**, *108*, 9048.
(29) Jin, H.; Li, X.; Maroncelli, M. *J. Phys. Chem. B* **2007**, *111*, 13473.
(30) Adhikari, A.; Sahu, A. K.; Dey, S.; Ghose, S.; Mandal, U.; Bhattacharyya, K. *J. Phys. Chem. B* **2007**, *111*, 12809.
(31) Hu, Z.; Margulis, C. J. *Proc. Natl. Acad. Sci. U.S.A.* **2006**, *103*, 831.
(32) Triolo, A.; Russina, O.; Fazio, B.; Appetecchi, G. B.; Carewska, M.; Passerini, S. *J. Chem. Phys.* **2009**, *130*, 164521.
(33) Horng, M. L.; Gardecki, J. A.; Papazyan, A.; Maroncelli, M. *J. Phys. Chem.* **1995**, *99*, 17311.
(34) Bhattacharyya, K.; Bagchi, B. *J. Phys. Chem. A* **2000**, *104*, 10603.
(35) Bhattacharyya, K. *Chem. Commun.* **2008**, 2848.
(36) Bhattacharyya, K. *Acc. Chem. Res.* **2003**, *36*, 95.
(37) Ghosh, S.; Mandal, U.; Adhikari, A.; Dey, S.; Bhattacharyya, K. *Int. Rev. Phys. Chem.* **2007**, *26*, 421.
(38) Biswas, R.; Rohman, N.; Pradhan, T.; Buchner, R. *J. Phys. Chem. B* **2000**, *112*, 9379.
(39) Bagchi, B.; Biswas, R. *Adv. Chem. Phys.* **1999**, *109*, 207.
(40) Biswas, R.; Bagchi, B. *J. Phys. Chem.* **1996**, *100*, 1238.
(41) Biswas, R.; Bagchi, B. *J. Phys. Chem.* **1999**, *103*, 2495.
(42) Kashyap, H.; Pradhan, T.; Biswas, R. *J. Chem. Phys.* **2006**, *125*, 174506.
(43) Sangma, P.; Mahiuddin, S.; Ismail, K. *J. Phys. Chem.* **1984**, *88*, 2378.
(44) Kalita, G.; Rohman, N.; Mahiuddin, S. *J. Chem. Eng. Data* **1998**, *43*, 148.
(45) Isard, J. O. *J. Non-Cryst. Solids* **1969**, *1*, 235.
(46) Day, D. E. *J. Non-Cryst. Solids* **1976**, *21*, 343.
(47) Dietzel, A. H. *Phys. Chem. Glasses* **1983**, *24*, 172.
(48) Moynihan, C. T. *J. Electrochem. Soc.* **1979**, *126*, 2144.
(49) Moynihan, C. T. In *Ionic Interactions*; Petrucci, S., Ed.; Academic Press: New York, 1971; Vol. 1.
(50) Chapman, C. F.; Maroncelli, M. *J. Phys. Chem.* **1991**, *95*, 9095.
(51) Dahl, K.; Biswas, R.; Ito, N.; Maroncelli, M. *J. Phys. Chem. B* **2005**, *109*, 1563.
(52) Pradhan, T.; Biswas, R. *J. Phys. Chem. A* **2007**, *111*, 11524.
(53) Pradhan, T.; Ghoshal, P.; Biswas, R. *J. Phys. Chem. A* **2008**, *112*, 915.
(54) Maroncelli, M.; Fleming, G. R. *J. Chem. Phys.* **1987**, *86*, 6221.
(55) Maroncelli, M. *J. Mol. Liq.* **1993**, *57*, 1.
(56) The average peak frequency is obtained by taking the arithmatic mean of the first moment of the spectrum and the peak value obtained by fitting the upper 40% of the spectrum to an inverted parabola (see for details: (a) Lewis, J. E.; Biswas, R.; Robinson, A. G.; Maroncelli, M. *J. Phys. Chem. B* **2001**, *105*, 3306. (b) Song, W.; Biswas, R.; Maroncelli, M. *J. Phys. Chem. A* **2000**, *104*, 6924.
(57) Jin, H.; Baker, G. A.; Arzhantsev, S.; Dong, J.; Maroncelli, M. *J. Phys. Chem. B* **2007**, *111*, 7291.
(58) Fee, R. S.; Maroncelli, M. *Chem. Phys.* **1994**, *183*, 235.
(59) Chapman, C. F.; Fee, R. S.; Maroncelli, M. *J. Phys. Chem.* **1995**, *99*, 4811.
(60) Horng, M. L.; Gardecki, J. A.; Maroncelli, M. *J. Phys. Chem. A* **1997**, *101*, 1030.
(61) Lakowicz, J. R. *Principles of Fluorescence Spectroscopy*, 2nd ed.; Kluwer Academic: New York, 1999.
(62) Cross, A. J.; Fleming, G. R. *Biophys. J.* **1984**, *46*, 45.
(63) Biswas, R.; Lewis, J. E.; Maroncelli, M. *Chem. Phys. Lett.* **1999**, *310*, 485.

(64) Pradhan, T.; Ghoshal, P.; Biswas, R. *J. Chem. Sci.* **2008**, *120*, 275.

(65) Since fluorescence emission in these highly viscous mixtures may not occur from the fully solvent-relaxed state, we have calculated the "actual" shift (steady state) by using the formula, $\Delta\Delta\nu = [\nu_{abs} - \nu_{em}(t=\infty)]^{mixture} - [\nu_{abs} - \nu_{em}]^{heptane}$, where the steady state emission frequency (ν_{em}) at each of the mixture compositions is replaced by the emission frequency obtained from the time-resolved measurements, $\nu_{em}(t=\infty)$. Note that $\Delta\Delta\nu$ calculated by using the above formula is essentially the dynamic Stokes' shift (Fee−Maroncelli method, ref 58), as $\nu_{em}^{mixture}(t=0) \approx \nu_{abs}^{mixture} - [\nu_{abs} - \nu_{em}]^{nonpolar}$. If one uses heptane as the nonpolar reference, then the Stokes' shift calculated from the above formula approximately equals the dynamic Stokes' shift ($\Delta\nu^t$) measured in time-resolved experiments.

(66) (a) Kashyap, H. K.; Biswas, R. *J. Phys. Chem. B* **2010**, *114*, 254. (b) Kashyap, H. K.; Biswas, R. *J. Phys. Chem. B* **2008**, *112*, 12431.

(67) Gray, C. G.; Gubbins, K. E. *Theory of Molecular Fluids*; Clarendon: Oxford, U.K., 1984; Vol. I.

(68) (a) Shirota, H.; Castner, E. W., Jr. *J. Am. Chem. Soc.* **2001**, *123*, 12877. (b) Chang, Y. J.; Castner, E. W., Jr. *J. Phys. Chem.* **1994**, *98*, 9712.

(69) Roy, S.; Bagchi, B. *J. Chem. Phys.* **1993**, *99*, 9938.

(70) (a) Nandi, N.; Roy, S.; Bagchi, B. *J. Chem. Phys.* **1995**, *102*, 1390. (b) Nandi, N.; Bagchi, B. *J. Phys. Chem.* **1996**, *100*, 13914.

(71) (a) Bart, E.; Meltsin, A.; Huppert, D. *J. Phys. Chem.* **1994**, *98*, 3295. (b) Bart, E.; Meltsin, A.; Huppert, D. *J. Phys. Chem.* **1994**, *98*, 10819.

(72) (a) Kashyap, H. K.; Biswas, R. *J. Chem. Phys.* **2007**, *127*, 184502. (b) Kashyap, H. K.; Biswas, R. *J. Chem. Sci.* **2007**, *119*, 391.

(73) (a) Marcus, Y.; Hefter, G. *Chem. Rev.* **2006**, *106*, 4585. (b) Marcus, Y.; Hefter, G. *Chem. Rev.* **2004**, *104*, 3405. (c) Hefter, G.; Marcus, Y.; Waghorne, W. E. *Chem. Rev.* **2002**, *102*, 2773. (d) Kalidas, C.; Hefter, G.; Marcus, Y. *Chem. Rev.* **2000**, *100*, 819.

(74) (a) Chandra, A.; Patey, G. N. *J. Chem. Phys.* **1994**, *100*, 1552. (b) Chandra, A. *Chem. Phys. Lett.* **1995**, *244*, 314. (c) Chandra, A.; Jana, D.; Bhattacharjee, S. *J. Chem. Phys.* **1996**, *104*, 8662. (d) Mahajan, K.; Chandra, A. *J. Chem. Phys.* **1997**, *106*, 2360.

(75) Bagchi, B. *Annu. Rev. Phys. Chem.* **1989**, *40*, 115.

(76) Bagchi, B.; Chandra, A. *Adv. Chem. Phys.* **1991**, *80*, 1.

(77) Funston, A. M.; Fadeeva, T. A.; Wishart, J. F.; Castner, E. W., Jr. *J. Phys. Chem. B* **2007**, *111*, 4963.

(78) Biswas, R.; Nandi, N.; Bagchi, B. *J. Phys. Chem. B* **1997**, *101*, 2968.

(79) The following expression for ion dynamic structure factor has been used to include the effects of inertial motion of ions on solvation energy relaxation: $S_{\alpha\beta}^{ion}(k;t) = S_{\alpha\beta}^{ion}(k)\exp\{-(k^2k_BT/m_\alpha\varsigma_\alpha^{ion})[t + (1/\varsigma_\alpha^{ion})(e^{-t\varsigma_\alpha^{ion}} - 1)]\}$, ς_α^{ion} being the translational friction on the αth type ion with mass m_α. ς_α^{ion} has been approximated by the Stokes' law and stick boundary condition for these ions.

(80) Chandrasekhar, S. *Rev. Mod. Phys.* **1943**, *14*, 180.

(81) Barthel, J.; Buchner, R.; Wurm, B. *J. Mol. Liq.* **2002**, *98−99*, 51.

(82) Ediger, M. D. *Annu. Rev. Phys. Chem.* **2000**, *51*, 99.

(83) Sillescu, H. *J. Non-Cryst. Solids* **1999**, *243*, 81.

(84) Ediger, M. D.; Angell, C. A.; Nagel, S. R. *J. Phys. Chem.* **1996**, *100*, 13200.

(85) Chang, I.; Fujara, F.; Geil, B.; Heuberger, G.; Mangel, T.; Sillescu, H. *J. Non-Cryst. Solids* **1994**, *172−174*, 248.

(86) Moynihan, C. T. *J. Phys. Chem.* **1966**, *70*, 3399.

(87) Angell, C. A. *J. Chem. Phys.* **1967**, *46*, 4673.

(88) Egelstaff, P. A. *An Introduction to the Liquid State*; Clarendon: Oxford, U.K., 1992.

(89) Pollack, G. L. *Phys. Rev. A* **1981**, *23*, 2660.

(90) Pollack, G. L.; Enyeart, J. J. *Phys. Rev. A* **1985**, *31*, 980.

(91) Voronel, A.; Veliyulin, E.; Machavariani, V. Sh.; Kisliuk, A.; Quitmann, D. *Phys. Rev. Lett.* **1998**, *80*, 2630.

(92) Evans, D. F.; Tominaga, T.; Davis, H. T. *J. Chem. Phys.* **1981**, *74*, 1298.

(93) Chen, S. H.; Davis, H. T.; Evans, D. F. *J. Chem. Phys.* **1981**, *75*, 1422.

(94) Chen, S. H.; Davis, H. T.; Evans, D. F. *J. Chem. Phys.* **1982**, *77*, 2540.

(95) Hiss, T. G.; Cussler, E. L. *AIChE J.* **1973**, *19*, 698.

(96) Diezemann, G.; Sillescu, H.; Hinze, G.; Bohmer, R. *Phys. Rev. E* **1998**, *57*, 4398.

(97) Jung, Y. J.; Garrahan, J. P.; Chandler, D. *Phys. Rev. E* **2004**, *69*, 061205−1.

(98) Ngai, K. L. *J. Phys. Chem. B* **1999**, *103*, 10684.

(99) Harris, K. R. *J. Chem. Phys.* **2009**, *131*, 054503.

(100) Shlesinger, M. F.; Zaslavsky, G. M.; Klafter, J. *Nature* **1993**, *363*, 31.

(101) Habasaki, J.; Ngai, K. L. *J. Chem. Phys.* **2008**, *129*, 194501.

(102) Hu, Z.; Huang, X.; Annapureddy, H. V. R.; Margulis, C. J. *J. Phys. Chem. B* **2008**, *112*, 7837.

(103) Ito, N.; Arzhantsev, S.; Heitz, M.; Maroncelli, M. *J. Phys. Chem. B* **2004**, *108*, 5771.

(104) Jin, H.; Baker, G. A.; Arzhantsev, S.; Dong, J.; Maroncelli, M. *J. Phys. Chem. B* **2007**, *111*, 7291.

(105) Paul, A.; Samanta, A. *J. Phys. Chem. B* **2007**, *111*, 4724.

(106) Paul, A.; Samanta, A. *J. Phys. Chem. B* **2008**, *112*, 947.

(107) (a) Seth, D.; Chakraborty, A.; Setua, P.; Sarkar, N. *J. Phys. Chem. B* **2007**, *111*, 4781. (b) Chakrabarty, D.; Seth, D.; Chakraborty, A.; Sarkar, N. *J. Phys. Chem. B* **2005**, *109*, 5753.

(108) Arzhantsev, S.; Jin, H.; Baker, G. A.; Maroncelli, M. *J. Phys. Chem. B* **2007**, *111*, 4978.

(109) Samanta, A. *J. Phys. Chem. B* **2006**, *110*, 13704.

(110) Mandal, P. K.; Samanta, A. *J. Phys. Chem. B* **2005**, *109*, 15172.

(111) Andreozzi, L.; Faetti, M.; Giordano, M.; Leporini, D. *J. Phys.: Condens. Matter* **1999**, *11*, A131.

(112) Andreozzi, L.; Bagnoli, M.; Faetti, M.; Giordano, M. *J. Non-Cryst. Solids* **2002**, *303*, 262.

(113) Andreozzi, L.; Di Schino, A.; Giordino, M.; Leporini, D. *Europhys. Lett.* **1997**, *38*, 669.

(114) Andreozzi, L.; Di Schino, A.; Giordino, M.; Leporini, D. *J. Phys.: Condens. Matter* **1996**, *8*, 9605.

(115) Andreozzi, L.; Faetti, M.; Giordino, M.; Leporini, D. *J. Phys. Chem. B* **1999**, *103*, 4097.

(116) Andreozzi, L.; Giordino, M.; Leporini, D. *J. Non-Cryst. Solids* **1998**, *235−237*, 219.

(117) Faetti, M.; Giordino, M.; Pardi, L.; Leporini, D. *Macromolecules* **1999**, *32*, 1876.

(118) Hooker, J. C.; Torkelson, J. M. *Macromolecules* **1995**, *28*, 7683.

(119) Dhinojwala, A.; Wong, G. K.; Torkeson, J. M. *J. Chem. Phys.* **1994**, *100*, 6046.

(120) Ye, J. Y.; Hattori, T.; Nakatsuka, H. *Phys. Rev. B* **1997**, *56*, 5286.

(121) Michele, D. C.; Leporini, D. *Phys. Rev. E* **2001**, *63*, 036702.

(122) Douglas, J. F.; Leporini, D. *J. Non-Cryst. Solids* **1998**, *235−237*, 137.

(123) Barkley, M. D.; Kowalczyk, A. A.; Brand, L. *J. Chem. Phys.* **1981**, *75*, 3581.

(124) Hu, Y.; Fleming, G. R. *J. Chem. Phys.* **1991**, *94*, 3857.

(125) Jas, G. S.; Larson, E. J.; Johnson, C. K.; Kuczera, K. *J. Phys. Chem. A* **2000**, *104*, 9841.

(126) Inamder, S. R.; Mannekutla, J. R.; Mulimani, B. G.; Savadatti, M. I. *Chem. Phys. Lett.* **2006**, *429*, 141.

(127) Tan, X.; Gustafson, T. L. *J. Phys. Chem. A* **2000**, *104*, 4469.

(128) Huang, W.; Richert, R. *Philos. Mag.* **2007**, *87*, 371.

(129) Cicerone, M. T.; Blackburn, F. R.; Ediger, M. D. *J. Chem. Phys.* **1995**, *102*, 471.

(130) Ingram, J. A.; Moog, R. S.; Ito, N.; Biswas, R.; Maroncelli, M. *J. Phys. Chem. B* **2003**, *107*, 5926.

(131) Because of our limited temporal resolution, dynamic Stokes' shift measurements could not be done at higher temperatures. However, it is logical to expect that $\langle\tau_s\rangle$ will track the solvent viscosity at higher temperatures in roughly the same manner as it has done at $T \sim 318$ K. The extent of heterogeneity will, of course, be much less at elevated temperatures and the enhanced fluidity will increase the long-time solvation rate. If it is considered that the solute−solvent nearest neighbor interactions, which is believed to be important for polar solvation dynamics at long-time,[39] also control substantially the solute rotation, then a similar proportionality relation between $\langle\tau_r\rangle$ and $\langle\tau_s\rangle$ can be expected at higher temperatures as well.

(132) Yang, M.; Richert, R. *Chem. Phys.* **2002**, *284*, 103.

(133) Fujisawa, T.; Nishikawa, K.; Shirota, H. *J. Chem. Phys.* **2009**, *131*, 244519.

(134) Turton, D. A.; Hunger, J.; Stoppa, A.; Hefter, G.; Thoman, A.; Walther, M.; Buchner, R.; Wynne, K. *J. Am. Chem. Soc.* **2009**, *131*, 11140.

(135) Attard, P. *Phys. Rev. E* **1993**, *48*, 3604.

(136) Chandra, A.; Bagchi, B. *J. Chem. Phys.* **1999**, *110*, 10024.

(137) Lebowitz, J. L. *Phys. Rev.* **1964**, *133*, A895.

JP1001176